AIAA AVIATION Forum
June 15-19, 2020, VIRTUAL EVENT
AIAA AVIATION 2020 FORUM

10.2514/6.2020-3138

Sensitivity Analysis for Aero-Thermo-Elastic Problems Using the Discrete Adjoint Approach

Soudeh Kamali[1], Dimitri J. Mavriplis[2], and Evan M. Anderson[3]
Department of Mechanical Engineering, University of Wyoming, Laramie, WY, 82070, USA

Coupled multidisciplinary sensitivity analysis is required for accurate design optimization in the simulation of many physical problems. Hence, in this work we look at the coupled thermo-elastic optimization capability of a finite-element solver developed in-house called AStrO. We validate AStrO's thermo-elastic sensitivity analysis and optimization capability by looking at multiple static and transient problems. Exact sensitivities calculated through the discrete adjoint method are presented for all the cases. Finally, the baseline and thermo-elastic optimization results for an aerodynamically heated panel case are used in an aero-thermo-elastic analysis. The aero-thermo-elastic analysis of this panel case shows how the thermo-elastic optimization of the panel modifies the flow solution. The in-house aero-thermo-elastic analysis platform used in this study was validated in previous work.

I. Nomenclature

L	=	objective function
D	=	design variables
u_S	=	state variables from the structure discipline
u_T	=	state variables from the thermal discipline
R_S	=	residual from the structure discipline
R_T	=	residual from the thermal discipline
Λ_S	=	adjoint from the structure discipline
Λ_T	=	adjoint from the thermal discipline
Ω	=	spatial domain of integration
R	=	residual
C	=	viscous damping matrix
M	=	mass matrix
K	=	stiffness matrix
T	=	temperature
Q	=	volumetric heat source
k	=	thermal conductivity
C	=	specific heat capacity
α	=	thermal expansion
E	=	Modulus of elasticity
v	=	Poisson's ratio
ρ	=	density
t	=	time
l	=	length of the geometry
u	=	displacement vector in a structure
$\dot{u}$	=	velocity vector in a structure
$\ddot{u}$	=	acceleration vector in a structure
T_0	=	initial temperature

[1] PhD Student, Department of Mechanical Engineering, AIAA Member.
[2] Professor, Department of Mechanical Engineering, AIAA Associate Fellow.
[3] PhD, Department of Wind Energy Technologies Sandia National Laboratory, AIAA Member.

u_i = vector displacement of a point in a structure
$\dot{u}_i$ = vector velocity of a point in a structure
$\ddot{u}_i$ = vector acceleration of a point in a structure
t_i = traction applied over the surface of a structure in vector form
ξ = damping coefficient
σ_i = stress at a point in a structure in vector form
ϵ_i = strain at a point in a structure in vector form
C_{ijkl} = elastic stiffness tensor
f_i = body force per unit volume at a point in a structure in vector form
N_{ij} = shape functions

II. Introduction

Most practical engineering problems involve interactions between various disciplines. Therefore, the computational design of such problems, must account for the coupling between the different disciplines. This coupling allows for each model to provide complementary information to the other, and therefore, eliminates many assumptions. An optimum multidisciplinary design is only reached after cycling between the different disciplines involved [1]. An important example of this type of problem is fluid-structure interaction. In recent years, the development of supercomputers has made simulation of coupled fluid-structure interactions possible. However, in many engineering designs it is not sufficient to just take into account the interaction of the fluid forces and structural deformations; temperature plays an important role as well [2, 3]. Hypersonic vehicles, for example, go through a wide range of flow conditions with large gradients of velocity and temperature close to their surface [4]. One of the major design concerns at these hypersonic velocities are high rates of heat transfer experienced by the vehicle [5]. Therefore, it is essential to account for the effect of temperature in order to obtain accurate numerical designs [6, 7].

The success of an aircraft design relies on the precise calculation of all the following: Aerodynamic loads (aerodynamic pressure and viscous forces), aero-thermal effects (surface heating rate and inner temperature distributions), and structural loads (structural deformation and stresses) [1, 8, 9]. Since the overall performance of an aeronautical system is governed in many cases by these coupling effects, the study of multidisciplinary optimization methods are of great importance [10]. The main challenge for these types of problems centers around the development of the corresponding disciplinary sensitivities and the coupling of them [11]. In many cases when dealing with coupled multidisciplinary simulations, one or more of the disciplines might be solved using low-fidelity models. However, in order to produce optimum designs, high-fidelity sensitivity analysis is preferred [12].

There are two main approaches to solving optimization problems: gradient-based and global search methods [13]. Gradient-based optimization methods are more popular within the field of aerodynamics. This is because of the lower number of analysis runs or function evaluation required for these methods in comparison to the global search techniques [14]. Gradient-based optimizations require the gradients of the objective function and constraints with respect to the design variables. These gradients are referred to as the sensitivity derivatives [15].

The finite-difference method is one of the simplest methods for computing the sensitivity derivatives. Although this approach is easy to implement, it is not the most efficient method. One problem with this approach is that it is computationally expensive, which makes it unsuitable for complex cases with many design variables [16]. Another problem is that the choice of the step size effects the accuracy of the gradient approximation [15]. Therefore, it would be better to calculate the sensitivities analytically. When calculating the sensitivity derivatives with the analytical approach, an additional level of simulation referred to as the sensitivity analysis, is required [15]. For sensitivity analysis a choice has to be made between the direct/tangent method and the adjoint method.

The adjoint approach has the advantage of computing cost function gradients at a cost independent of the number of design variables [16]. This characteristic makes the adjoint method extremely efficient for high-fidelity, multidisciplinary design problems [11, 17-19]. For such problems, the discrete adjoint is highly favored since it follows the discretization of the governing equations naturally and enables a methodical approach for obtaining the sensitivities for any arbitrarily complex analysis procedure [14, 20, 21].

In this work we study the multidisciplinary sensitivity analysis and optimization for thermo-elastic problems using a finite-element solver developed in-house. We also use the aero-thermo-elastic analysis platform developed and validated in reference [22] to further study the effect of the thermo-elastic optimization on the flow solution of an aerodynamically heated panel case. The premise of the current work is that a modern multidisciplinary design optimization must include high-fidelity models for all the disciplines involved.

This paper is structured as follows. Section III gives more detail on the previously developed aero-thermo-elastic coupling platform by taking a look at each of the required components and the governing equations of each discipline. Section IV briefly presents the equations that are used to obtain the thermo-elastic sensitivities in the structural solver used in this study. Section V provides validation results for the static and transient thermo-elastic sensitivity and optimization capability of the structural solver. In section VI we compare aero-thermo-elastic analysis solution for a baseline and thermo-elastically optimized transient aerodynamically heated panel case. Section VII draws conclusions and highlights future work.

III. Aero-Thermo-Elastic Analysis Coupling

Generally, when approaching a multidisciplinary simulation, there are two options available: strong and weak coupling. In the first case, the flow, elasticity and heat transfer equations are treated as one single system of equations and solved at once using a single numerical framework. In the second case, the solution of each discipline is obtained from independent codes and then coupled together by exchanging boundary conditions at the interface between the domains [23, 24]. The strong coupling approach is the more stable approach; however, it suffers from the inability to use already available and well-tested solvers. On the other hand, the weak coupling approach is able to use existing, well-developed and tested codes for each discipline. This approach does however have its own disadvantages. These are: the problem of stability and the difficulty of transferring data between the individual disciplinary codes [25, 26].

The code-coupling can be very challenging in practice. The two main challenges, which arise from the discontinuities between the models, are: time-scale discontinuity, and space-scale discontinuity [7, 27]. In the following pages we will explain how we dealt with each of these challenges in developing our in-house aero-thermo-elastic analysis platform. A detailed description of the aero-thermo-elastic analysis platform is given in reference [22]. This platform couples the three disciplines through a weak coupling approach. This decision was made to allow us to take advantage of the already available and tested high-fidelity flow solver and structural solver developed in-house for multidisciplinary modeling and optimization.

Figure 1 summarizes the transfer of information for the aero-thermo-elastic analysis process. Figure 2 illustrates the procedure for the weak coupling strategy used in this aero-thermo-elastic platform. In the rest of this section we briefly look at the different components of the numerical set up required to run an aero-thermo-elastic analysis simulation: the flow solver, the structural solver (elasticity and thermal equation), fluid-structure interaction (FSI) module, and the mesh deformation capability.

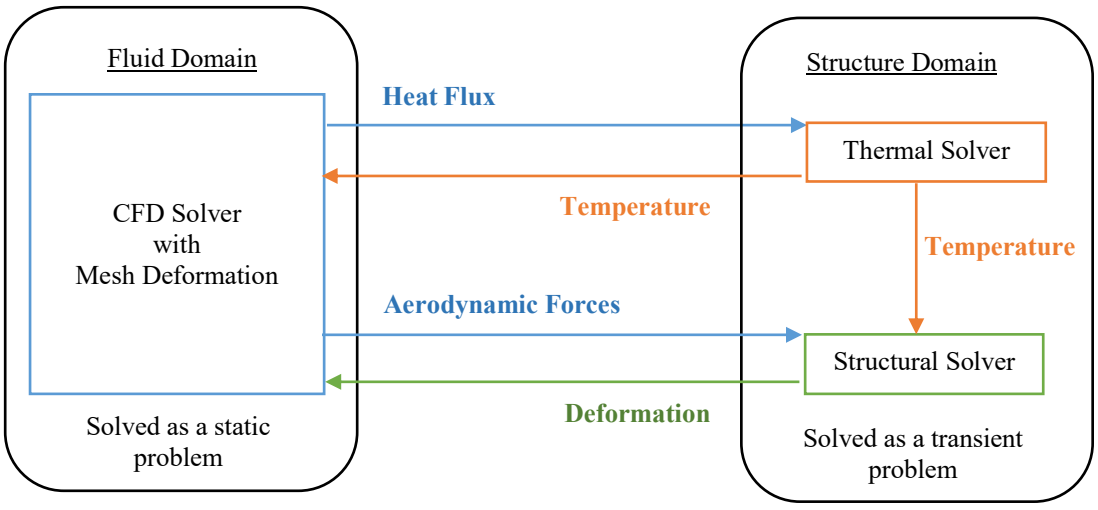

Fig. 1 Transfer of information for the coupled aero-thermo-elastic analysis platform.

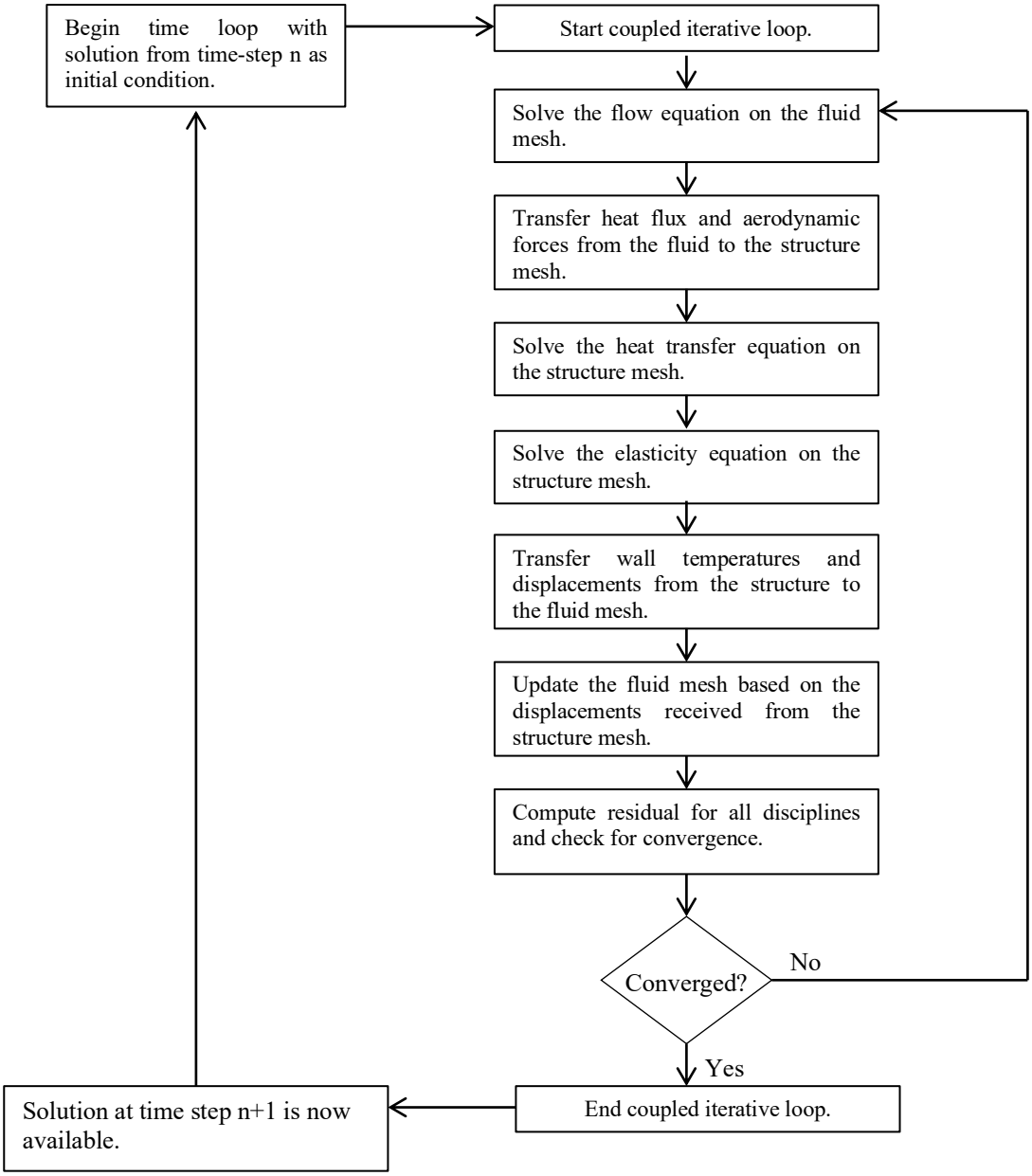

Fig. 2 Iterative loop for advancing from time-step n to time-step n+1 in the aero-thermo-elastic analysis problem with weak coupling.

A. Flow Solver

The flow solver used in this study is the "Navier-Stokes Unstructured 3D" (NSU3D) code, which is a Reynolds-averaged Navier-Stokes (RANS) solver for unstructured grids [17]. It is a vertex-centered finite volume solver, which is second-order in both time and space. This flow solver uses a line-implicit agglomeration multigrid algorithm, which can be used either as a non-linear solver, or a linear solver within an approximate Newton method, or as a pre-conditioner for GMRES for driving the non-linear steady-state residual to zero [28]. For time-dependent problems, all the above-mentioned solvers can be used in a dual-time stepping approach for solving the non-linear problem, which arises at each time step [29]. NSU3D has been widely validated for both steady state and time-dependent flow problems, having been used in numerous simulations and participations in events such as the Drag Prediction Workshop, the High-Lift Prediction Workshop, and the Aero-elastic Prediction Workshop series [30-33].

More recently, NSU3D has been extended for use in coupled aero-elastic calculations [14, 29, 34, 35] and high-speed aero-thermo-elastic simulations [22] . Detailed explanation of this solver can be found in available previous references [17, 36, 37]. As such, only a concise description of the formulations will be given in this paper.

The flow solver is based on the conservative form of the Navier-Stokes equations. These may be written as:

$$\frac{\partial u(x,t)}{\partial t} + \nabla . F(u) = 0 \tag{1}$$

For moving mesh problems, the above formulation is written in arbitrary Lagrangian-Eulerian (ALE) form, as:

$$\frac{\partial Vu}{\partial t} + \int_{B(t)} [F(u) - \dot{x}u] . ndB = 0 \tag{2}$$

here V refers to the volume of the control volume bounded by a control surface $B(t)$, $\dot{x}$ is the vector of mesh face or edge velocities, and n is the unit normal of the face or edge. Vector u denotes the state vector of conserved variables, and the flux vector F contains both inviscid and viscous fluxes. The equations are closed with the perfect gas equation of state for cases presented in this work [14, 36].

The time derivative term is discretized using a second-order accurate backward difference formula (BDF2) scheme, leading to the implicit system of equations at each time step given as:

$$\frac{3}{2\Delta t} V^n u^n - \frac{2}{\Delta t} V^{n-1} u^{n-1} + \frac{1}{2\Delta t} V^{n-2} u^{n-2} + S^n(u^n, x^n, \dot{x}^n) = 0 \tag{3}$$

where $V^n = V(x^n)$ represents the mesh control volumes and $S^n(u^n, x^n, \dot{x}^n)$ represents the spatial discretization terms at the n^{th} time step.

The functional dependence of the implicit system to be solved at each time step can be written in residual form as:

$$R^n(u^n, u^{n-1}, u^{n-2}, x^n, x^{n-1}, x^{n-2}) = 0, \quad n = ,2,3, \dots, N \tag{4}$$

where the initial conditions are given by u^0 and x^0, and noting that a BDF1 time discretization is used for the first time step.

At each time step, the implicit residual is solved using a line-implicit solver with agglomeration multigrid. The fluxes are calculated using the Roe scheme [38] and a Barth Jespersen limiter [39] is applied to the cases presented in this work.

Considerable effort has been spent in previous work for implementing and verifying the discrete adjoint approach for computing sensitivities within the NSU3D unstructured mesh RANS CFD solver. Exact sensitivities can be calculated for both steady-state and time-dependent problems in the NSU3D framework using the adjoint and tangent methods [29, 37, 40].

B. Structural Solver

The structural solver used in this study is a finite-element solver named AStrO (Adjoint-based Structural Optimizer), which was developed in-house. AStrO has been introduced in previous work [14, 22, 29, 34, 35] and supports both linear and nonlinear finite-element modeling of three-dimensional structures [34]. AStrO also supports finite element modeling of thermo-elastic behavior of structures. AStrO can run static or dynamic analysis of either the heat transfer problem, or the elasticity problem, or the two coupled disciplines [41]. The motivation for constructing an in-house structural solver was to have the capability of doing analysis and calculating sensitivities for coupled CFD and computational thermal and structural dynamics (CTSD) problems [14] .

AStrO is compatible with existing commercial structural analysis software tools such as Abaqus [42]. It contains an interface that can process model input files generated by Abaqus [29]. Dynamic systems are modeled with implicit second-order accurate time integration by the Hilber-Hughes-Taylor “alpha” method, which is a variation of the Newmark Beta method [43]. The discretized equations for the elasticity problem are derived from the widely used virtual work formulation [43]. The temperature distribution due to heat conduction through a structure is governed by the Poisson equation, which is discretized in a similar manner as the equations of elasticity. In the following paragraphs we take a closer look at AStrO’s governing equations.

The transient elasticity equation solved in AStrO is given as:

$$\nabla \cdot \sigma - \xi \frac{du}{dt} - \rho \frac{d^2u}{dt^2} + f = 0 \tag{5}$$

where f represents the applied body forces, u is the vector of displacements, σ is the stress tensor, and ξ is the damping coefficient.

The principle of virtual work applied to the equations of elasticity for a deformable elastic body subject to applied body forces and surface tractions, as well as damping forces proportional to velocity, can be expressed mathematically as:

$$\int_\Omega (\sigma \cdot \delta\epsilon) d\Omega + \int_\Omega \xi(\dot{u} \cdot \delta u) d\Omega + \int_\Omega \rho(\ddot{u} \cdot \delta u) d\Omega - \int_\Omega (f \cdot \delta u) d\Omega - \int_S (t \cdot \delta u) dS = 0 \tag{6}$$

In the above u, $\dot{u}$, $\ddot{u}$ are the vector displacement, velocity, and acceleration at a point in a structure, σ and ϵ are the stress and strain in second-order tensor form, ξ is the damping coefficient, ρ is the mass density, f is the applied body force per unit volume, and t is the applied surface traction per unit area on the structure. The final term is the integral of traction over the surface area of the structure, while all other terms are volume integrals over the body of the structure. The δ operator indicates a variation on the function to its right, meaning the above must hold for any variation of the displacement field u [34, 41]. The virtual displacement, δu, is a function of space throughout the body, and $\delta\epsilon$ is the variation of strain corresponding to that virtual displacement.

The equation of motion for dynamic elastic bodies derived from the principle of virtual work discretized using the finite element method is:

$$\int_\Omega \sigma_i \frac{\partial \epsilon_i}{\partial U_j} d\Omega + \int_\Omega \xi \dot{u}_i N_{ij} d\Omega + \int_\Omega \rho \ddot{u}_i N_{ij} d\Omega - \int_\Omega f_i N_{ij} d\Omega - \int_S t_i N_{ij} dS = 0 \tag{7}$$

where N_{ij} is a matrix of basis functions and U_j is a vector of nodal solution parameters, or degrees of freedom. The matrix equivalent of Eq. (7) is then obtained as shown in Eq. (8):

$$KU + C\dot{U} + M\ddot{U} = F \tag{8}$$

where K is the stiffness matrix, M is the mass matrix, C is the viscous damping matrix, F is the vector of forces, U is the vector of nodal values of displacements, $\dot{U}$ vector of nodal values of velocities, and $\ddot{U}$ vector of nodal values of acceleration.

The transient heat equation solved in AStrO is given as:

$$\rho c \frac{\partial T}{\partial t} + \nabla \cdot (k \nabla T) - Q = 0 \tag{9}$$

where, Q is the rate of internal heat generation per unit volume, k is the thermal conductivity, c is the specific heat capacity, ρ the density, and T is the temperature.

The variational form for temperature distribution due to heat conduction in a structure can be developed in a similar fashion as the equations of elasticity:

$$-\int_\Omega \big(q \cdot \delta(\nabla T)\big) d\Omega + \int_\Omega \rho C_p \dot{T} \delta T d\Omega - \int_\Omega Q \delta T d\Omega + \int_S (q \cdot n) \delta T dS = 0 \tag{10}$$

The discretized governing equations for heat conduction in structures derived from the variational form using the finite element method is:

$$-\int_\Omega q_i \frac{\partial N_j}{\partial x_i} d\Omega + \int_\Omega \rho C_p \dot{T} N_j d\Omega - \int_\Omega Q N_j d\Omega + \int_S q_i n_i N_j dS = 0 \tag{11}$$

where n_i is the normal vector, q_i is the surface heat flux, and N_j the basis function.

The matrix equivalent is then obtained as shown in Eq. (12):

$$K_{therm}T + M_{therm}\dot{T} = F_{therm} \tag{12}$$

where T is the nodal values of temperature, K_{therm} is the global thermal conductivity matrix, M_{therm} is the thermal mass matrix, and F_{therm} is the internal heat generation.

AStrO is capable of modeling the coupled thermo-elastic responses in structures. However, there are several simplifying assumptions made. The first assumption is that thermal material properties such as conductivity and specific heat capacity have no significant dependence on strain. Furthermore, the heat generated by deformation is assumed to be negligible. In other words, the deformation has a one-way dependence on the temperature distribution. These assumptions are acceptable, since the cases to be considered are expected to have small values of strain and within the elastic regime, selected materials will have low internal damping characteristics, and deformation rates will not produce significant heat through phenomena such as viscoelasticity [41].

Under these assumptions, in any given analysis, the temperature distribution of a structure can be obtained first, followed by the deformation solution based on the temperature results in addition to applied loads. To account for the dependence of deformation on the temperature distribution, an adjustment to the definition of total strain is required. Any point in the structure that is subject to a combination of applied stress and change in temperature will exhibit a measure of strain for each of those contributors. Hence, the total strain can be expressed as:

$$\epsilon_i^{total} = \epsilon_i^{stress} + \epsilon_i^{therm} \tag{13}$$

In the governing equations of elasticity based on the principle of virtual work, stress at a point under the assumption of linear elasticity can be expressed as:

$$\sigma_i = C_{ik}\epsilon_k \tag{14}$$

where C_{ik} is the stiffness matrix of the local material. However, ϵ_k in Eq. (14) must only be the strain due to the applied stress. Therefore, in the presence of thermal expansions, we have:

$$\sigma_i = C_{ik}\epsilon_k^{stress} = C_{ik}\left(\epsilon_k^{total} - \epsilon_k^{therm}\right) \tag{15}$$

The strain due to thermal expansion is assumed to be linearly related to temperature, such that the change in temperature from some reference temperature T^{ref} multiplied by a vector of thermal expansion coefficients α gives the resulting thermal strain to be:

$$\epsilon_k^{therm} = (T - T^{ref})\alpha_k = \Delta T \alpha_k \tag{16}$$

If the stress in Eq. (7) is expressed using Eq. (15) and Eq. (16), then the governing equations for the elastic response taking into account the change in temperature, becomes:

$$\int_\Omega C_{ik}\left(\epsilon_k^{total} - \Delta T\alpha_k\right)\frac{\partial \epsilon_i}{\partial U_j}d\Omega + \int_\Omega \xi \dot{u}_i N_{ij}d\Omega + \int_\Omega \rho \ddot{u}_i N_{ij}d\Omega - \int_\Omega f_i N_{ij}d\Omega - \int_S t_i N_{ij}dS = 0 \tag{17}$$

Since the temperature solution is pre-computed, the effect of thermal expansion shows up as part of the load in the elasticity equations [41].

AStrO has the capability of calculating exact sensitivities using the adjoint method [34] and it has been coupled with NSU3D for Aero-elastic sensitivity analysis and optimization in previous work [14, 29, 34, 41]. AStrO also offers an on-board optimizer using the steepest-descent line search algorithm with backtracking [44]. This function is convenient for simple problems and for trouble shooting, since it does not require linking with external packages. This optimizer was used for all the thermo-elastic optimization results presented in this paper. Alternatively, more sophisticated optimizers can be linked to AStrO for more complex optimization problems [41].

C. Fluid-Structure Interaction (FSI)

Proper data transfer between different disciplines is one of the most important factors in multidisciplinary analysis and design. Correct modeling of aero-thermo-elastic problems requires an accurate coupling of the fluid and structure codes. Although in these problems the geometry is shared, the models most often have dissimilar meshes. Moreover, some of the data from one domain is usually needed to be available on the other domain [45]. The weak coupling method uses an iterative approach to calculate the same temperature and heat flux at the boundaries of the fluid and structure domain. Likewise, it checks to see if the values for the aerodynamic loads on the fluid side and the displacements generated by the structure solver in response to these aerodynamic loads, have converged. The computation alternates between the fluid and structure domains with exchange of the above-mentioned boundary conditions [46, 47]. In weak coupled codes, the CFD and CTSD codes are alternatively called from a master program. This master program is also in charge of transferring data between the codes on the CFD/CTSD interface.

In order to control the stability and convergence in these problems, the choice of the boundary condition is very important. In the literature, the continuity of temperature and heat flux at the interface is mainly implemented by imposing the wall temperature distribution computed from the CTSD solution on the fluid side and the heat flux distribution computed from the CFD solution on the structure side. This method is known as the flux forward temperature back (FFTB) method or the Dirichlet-Neumann boundary condition. Many researchers have shown that the use of this type of boundary condition is the key to achieving numerical stability and having robust convergence [46-49].

An FSI module had previously been created in-house and used for aero-elastic analysis and design [14, 29]. This model was able to successfully transfer the aerodynamic forces from the fluid solver to the structure solver, and in return pass the calculated displacements to the fluid surface mesh [29]. This module was updated so that it can also transfer temperature and heat flux between the fluid and structure meshes [22] . When dealing with the aero-thermo-elastic analysis, we need to exchange the aerodynamic forces and heat fluxes from the fluid domain to the structure domain, and in return send the temperatures and displacements from the structure mesh to the fluid mesh. The effects of the temperature on the structure are dealt with internally in the structure code as explained in the previous section.

In practice the FSI computes the heat fluxes and the aerodynamic forces at each CFD surface mesh point. These values are then projected onto the finite-element basis functions where they are assembled in the form of heat fluxes and forces on the finite-element nodal locations. Conversely, once the structural temperature and displacement solutions have been computed, they are transferred back to the surface CFD mesh in a similar manner [14]. This transfer of data between the two meshes can be summarized with the following equations:

$$\begin{cases} Q_{CTSD} = [P]Q_{CFD} \\ T_{CFD} = [P]^T T_{CTSD} \end{cases} \tag{18}$$

$$\begin{cases} F_{CTSD} = [P]F_{CFD} \\ U_{CFD} = [P]^T U_{CTSD} \end{cases} \tag{19}$$

where [P] represents the rectangular transfer matrix which projects pointwise CFD surface heat fluxes and forces onto the individual structure mesh surface points. The transpose of the matrix is used to obtain the CFD surface temperatures and displacements from the structure mesh [29]. The interpolation patterns which define the [P] matrix are computed by locating the perpendicular projection of each point of the surface CFD mesh on the structure model elements [14]. This is done through a fast parallel search technique, which is based on the minimum distance search [50].

It should be mentioned here that the in-house developed FSI is capable of working with non-matching fluid and structure meshes with different element types and mesh resolution. Moreover, the developed FSI has the ability to handle fluid and structure models that have non-matching outer-mold line (OML) geometries [29]. Additionally, the FSI formulation is discretely conservative for the transfer of forces and heat fluxes from the fluid to the structure and satisfies the principle of conservation of virtual work for the transfer of displacements from the structure to the fluid.

D. Mesh Deformation

When dealing with aero-thermo-elastic problems, we require a mesh deformation capability in order to account for the displacements computed by the structural solver in response to the aerodynamic and thermal loads. When running time-dependent problems, we may also have prescribed surface deflections at certain times, such as when simulating prescribed motion of a control surface. Hence, the CFD solver needs to be modified to take into account the additional dynamics introduced due to the mesh motion, and the fluid equations must be written in the ALE

framework [51, 52]. NSU3D employs a discretization that respects the Geometric Conservation Law (GCL) [53] to make sure the flow solver keeps its accuracy and stability in the presence of arbitrary mesh motion. Significant work has been done in the past on the development of a robust and efficient mesh deformation technique [54, 55]. This approach is based on the linear elasticity model and the mesh deformation equations are discretized using a second-order accurate continuous Galerkin finite-element approach [29]. The equations for the mesh deformation are solved using the same line-implicit multigrid algorithm used for solving the flow equations [32].

IV. Thermo-Elastic Sensitivity Formulation for Structural Solver

In this section we look at both the static and transient thermo-elastic sensitivity analysis formulation in AStrO. First, general formulations are presented and later these formulations are updated taking into account the specifics of AStrO. We also look briefly at the complex-step method used to validate the sensitivities calculated by the tangent and adjoint method in this work.

A. Static Thermo-Elastic Sensitivity Analysis Formulation

For gradient-based optimization, sensitivities of the objective with respect to the design parameters are required. Consider an objective function such as L:

$$L = L(D, u_T(D), u_s(D)) \tag{20}$$

As shown in Eq. (20) above, in addition to an explicit dependence on the design inputs D, there exists an implicit dependence through the state variables u_T, u_S, coming from the thermal and structure disciplines respectively. In all the following equations the subscripts T, and *S* refer to the thermal and structure disciplines respectively. Using the chain rule, the sensitivity of the objective function with respect to the design variables D can be expressed as:

$$\frac{dL}{dD} = \frac{\partial L}{\partial D} + \frac{\partial L}{\partial u_T}\frac{\partial u_T}{\partial D} + \frac{\partial L}{\partial u_S}\frac{\partial u_S}{\partial D} \tag{21}$$

The above equation can also be expressed as:

$$\frac{dL}{dD} = \frac{\partial L}{\partial D} + \begin{bmatrix}\frac{\partial L}{\partial u_T} & \frac{\partial L}{\partial u_S}\end{bmatrix}\begin{bmatrix}\frac{\partial u_T}{\partial D} \\ \frac{\partial u_S}{\partial D}\end{bmatrix} \tag{22}$$

The linearization of the objective function with respect to the disciplinary state variables can easily be computed. However, the linearization of the disciplinary state variables with respect to the design variables are unknown quantities at this point and an expression for their evaluation must be determined. The governing nonlinear equations of each discipline in residual form are:

$$R_T(D, u_T, u_S) = 0 \tag{23}$$

$$R_S(D, u_T, u_S) = 0 \tag{24}$$

As can be seen from Eq. (23) and Eq. (24) above, the residual equation from each discipline not only depends on its own state variables but also on the state variables of the other discipline. This is because of the assumption of coupling between the disciplines. Since we are assuming a general case here, the residual equation will also have dependence on the design variables D. Differentiating the disciplinary residual equations with respect to the set of design variables D yields:

$$\frac{\partial R_T}{\partial D} + \frac{\partial R_T}{\partial u_T}\frac{\partial u_T}{\partial D} + \frac{\partial R_T}{\partial u_S}\frac{\partial u_S}{\partial D} = 0 \tag{25}$$

$$\frac{\partial R_S}{\partial D} + \frac{\partial R_S}{\partial u_T}\frac{\partial u_T}{\partial D} + \frac{\partial R_S}{\partial u_S}\frac{\partial u_S}{\partial D} = 0 \tag{26}$$

As mentioned previously, AStrO assumes a one-way dependence of elastic displacement on temperature distribution for thermo-elastic analysis. This means that Eq. (25) can be further simplified as follows:

$$\frac{\partial R_T}{\partial u_S} = 0 => \frac{\partial R_T}{\partial D} + \frac{\partial R_T}{\partial u_T}\frac{\partial u_T}{\partial D} = 0 \tag{27}$$

Equations (25), and (27) can be combined into matrix form as shown in Eq. (28).

$$\begin{bmatrix} \frac{\partial R_T}{\partial u_T} & 0 \\ \frac{\partial R_S}{\partial u_T} & \frac{\partial R_S}{\partial u_S} \end{bmatrix} \begin{bmatrix} \frac{\partial u_T}{\partial D} \\ \frac{\partial u_S}{\partial D} \end{bmatrix} = \begin{bmatrix} -\frac{\partial R_T}{\partial D} \\ -\frac{\partial R_S}{\partial D} \end{bmatrix} \tag{28}$$

Solving the above set of equations using disciplinary forward substitution provides us with the state variable sensitivities with respect to the design variables. Now we can replace this into Eq. (21) and solve for the complete sensitivity vector $\frac{dL}{dD}$.

When calculating sensitivities with the above (tangent) method, the linearization scales directly with the number of design variables. Since the number of design variables is usually large, the adjoint procedure is used as a more efficient way of calculating these sensitivities. The adjoint method is the more efficient method since the cost of this method is independent of the number of design parameters [34].

For the adjoint formulation we require the transpose of the forward linearization as shown below:

$$\frac{dL}{dD}^T = \frac{\partial L}{\partial D}^T + \begin{bmatrix} \frac{\partial u_T}{\partial D}^T & \frac{\partial u_S}{\partial D}^T \end{bmatrix} \begin{bmatrix} \frac{\partial L}{\partial u_T}^T \\ \frac{\partial L}{\partial u_S}^T \end{bmatrix} \tag{29}$$

In the adjoint method the computation of the state variable sensitivities is avoided. The following expression is obtained for the state variable sensitivities by transposing and rearranging Eq. (28):

$$\begin{bmatrix} \frac{\partial u_T}{\partial D}^T & \frac{\partial u_S}{\partial D}^T \end{bmatrix} = \begin{bmatrix} -\frac{\partial R_T}{\partial D}^T & -\frac{\partial R_S}{\partial D}^T \end{bmatrix} \begin{bmatrix} \frac{\partial R_T}{\partial u_T}^T & \frac{\partial R_S}{\partial u_T}^T \\ 0 & \frac{\partial R_S}{\partial u_S}^T \end{bmatrix}^{-1} \tag{30}$$

Substituting the above into Eq. (29), yields:

$$\frac{dL}{dD}^T = \frac{\partial L}{\partial D}^T + \begin{bmatrix} -\frac{\partial R_T}{\partial D}^T & -\frac{\partial R_S}{\partial D}^T \end{bmatrix} \begin{bmatrix} \frac{\partial R_T}{\partial u_T}^T & \frac{\partial R_S}{\partial u_T}^T \\ 0 & \frac{\partial R_S}{\partial u_S}^T \end{bmatrix}^{-1} \begin{bmatrix} \frac{\partial L}{\partial u_T}^T \\ \frac{\partial L}{\partial u_S}^T \end{bmatrix} \tag{31}$$

The adjoint variable for each discipline is defined as:

$$\begin{bmatrix} \Lambda_T \\ \Lambda_S \end{bmatrix} = \begin{bmatrix} \frac{\partial R_T}{\partial u_T}^T & \frac{\partial R_S}{\partial u_T}^T \\ 0 & \frac{\partial R_S}{\partial u_S}^T \end{bmatrix}^{-1} \begin{bmatrix} \frac{\partial L}{\partial u_T}^T \\ \frac{\partial L}{\partial u_S}^T \end{bmatrix} \tag{32}$$

The coupled linear adjoint system of equations in AStrO is then:

$$\begin{bmatrix} \frac{\partial R_T}{\partial u_T}^T & \frac{\partial R_S}{\partial u_T}^T \\ 0 & \frac{\partial R_S}{\partial u_S}^T \end{bmatrix} \begin{bmatrix} \Lambda_T \\ \Lambda_S \end{bmatrix} = \begin{bmatrix} \frac{\partial L}{\partial u_T}^T \\ \frac{\partial L}{\partial u_S}^T \end{bmatrix} \tag{33}$$

To solve for the vector of adjoint variables in Eq. (33), a back substitution needs to be performed.

Once the vector of adjoint variables for each discipline is available, it may be substituted into the total sensitivity equation as:

$$\frac{dL}{dD}^T = \frac{\partial L}{\partial D}^T + \begin{bmatrix} -\frac{\partial R_T}{\partial D}^T & -\frac{\partial R_S}{\partial D}^T \end{bmatrix} \begin{bmatrix} \Lambda_T \\ \Lambda_S \end{bmatrix} \tag{34}$$

It is clear from the above equations that the number of design variables only affects the matrix-vector products at the end of the computation process [56]. This is why the adjoint method is more efficient in calculating sensitivities than the tangent method. In this work, both the tangent and adjoint methods are implemented and compared.

When dealing with thermo-elastic sensitivity analysis we also need to transfer sensitivities between the thermal and structure domains. The transfer of information for the sensitivity analysis process done by AStrO for the tangent and adjoint method are summarized in Fig. 3. The one-way dependence between the elastic displacement on temperature distribution is clear in this figure.

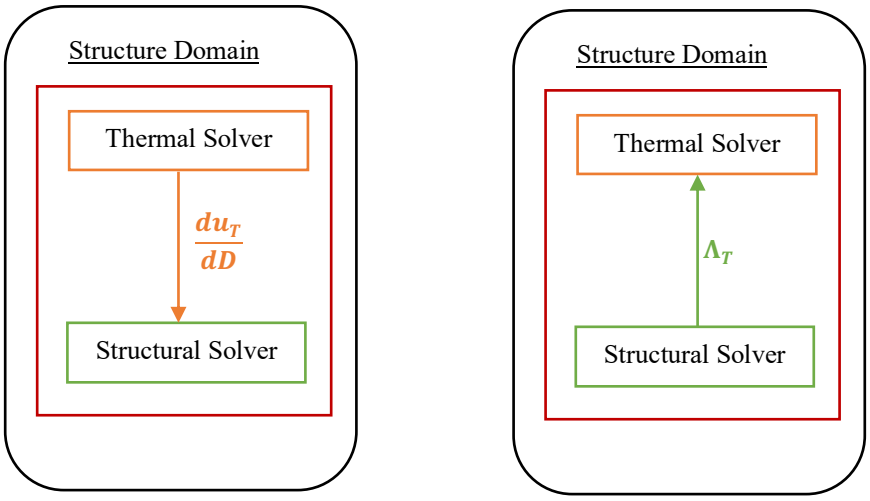

Fig. 3 Flow of information for the thermo-elastic tangent (on the left) and Adjoint (on the right) sensitivity analysis process in AStrO.

B. Transient Thermo-Elastic Sensitivity Analysis Formulation

For transient simulations, the Jacobian matrices $\frac{\partial R}{\partial u}$, span in both the spatial and temporal domains. Since time is purely hyperbolic in nature, the discrete residual R at any arbitrary time step n can only depend on quantities at time indices $\leq n$. Therefore, the discrete time expansion of any Jacobian matrix for a temporal domain consisting of n time steps, results in a block lower triangular matrix as shown in Eq. (35). In this form, each of the blocks is a matrix spanning the spatial domain. The matrix is lower triangular with one non-zero off-diagonal block, resulting from the dependence of the Newmark Beta time stepping scheme on only the previous time level.

$$\frac{\partial R}{\partial u} = \begin{bmatrix} \frac{\partial R^0}{\partial u^0} & 0 & 0 & 0 & \dots \\ \frac{\partial R^1}{\partial u^0} & \frac{\partial R^1}{\partial u^1} & 0 & 0 & \dots \\ 0 & \frac{\partial R^2}{\partial u^1} & \frac{\partial R^2}{\partial u^2} & 0 & \dots \\ 0 & 0 & \frac{\partial R^3}{\partial u^2} & \frac{\partial R^3}{\partial u^3} & \dots \\ \vdots & \vdots & \vdots & \vdots & \ddots \end{bmatrix} \tag{35}$$

Now, for the thermo-elastic problem, let us assume a temporal domain consisting of two time-steps *n* and *n – 1*. Hence, Eq. (28) can be rewritten using the discrete temporal expansion of the Jacobian matrices as:

$$\left[\begin{array}{cc|cc} \frac{\partial {R_T}^{n-1}}{\partial {u_T}^{n-1}} & 0 & \frac{\partial {R_T}^{n-1}}{\partial {u_S}^{n-1}} & 0 \\ \frac{\partial {R_T}^{n}}{\partial {u_T}^{n-1}} & \frac{\partial {R_T}^{n}}{\partial {u_T}^{n}} & \frac{\partial {R_T}^{n}}{\partial {u_S}^{n-1}} & \frac{\partial {R_T}^{n}}{\partial {u_S}^{n}} \\ \hline \frac{\partial {R_S}^{n-1}}{\partial {u_T}^{n-1}} & 0 & \frac{\partial {R_S}^{n-1}}{\partial {u_S}^{n-1}} & 0 \\ \frac{\partial {R_S}^{n}}{\partial {u_T}^{n-1}} & \frac{\partial {R_S}^{n}}{\partial {u_T}^{n}} & \frac{\partial {R_S}^{n}}{\partial {u_S}^{n-1}} & \frac{\partial {R_S}^{n}}{\partial {u_S}^{n}} \end{array}\right] \left[\begin{array}{c} \frac{\partial {u_T}^{n-1}}{\partial D} \\ \frac{\partial {u_T}^{n}}{\partial D} \\ \hline \frac{\partial {u_S}^{n-1}}{\partial D} \\ \frac{\partial {u_S}^{n}}{\partial D} \end{array}\right] = \left[\begin{array}{c} -\frac{\partial {R_T}^{n-1}}{\partial D} \\ -\frac{\partial {R_T}^{n}}{\partial D} \\ \hline -\frac{\partial {R_S}^{n-1}}{\partial D} \\ -\frac{\partial {R_S}^{n}}{\partial D} \end{array}\right] \tag{36}$$

The overall system can be represented as a block lower triangular matrix by swapping the rows and columns as shown in Eq. (37). The one-way dependence of elastic displacement on temperature distribution for thermo-elastic analysis in AStrO has been taken into account in Eq. (37) below. In this form, each diagonal block represents a single time step.

$$\left[\begin{array}{cc|cc} \frac{\partial {R_T}^{n-1}}{\partial {u_T}^{n-1}} & 0 & 0 & 0 \\ \frac{\partial {R_S}^{n-1}}{\partial {u_T}^{n-1}} & \frac{\partial {R_S}^{n-1}}{\partial {u_S}^{n-1}} & 0 & 0 \\ \hline \frac{\partial {R_T}^{n}}{\partial {u_T}^{n-1}} & 0 & \frac{\partial {R_T}^{n}}{\partial {u_T}^{n}} & 0 \\ \frac{\partial {R_S}^{n}}{\partial {u_T}^{n-1}} & \frac{\partial {R_S}^{n}}{\partial {u_S}^{n-1}} & \frac{\partial {R_S}^{n}}{\partial {u_T}^{n}} & \frac{\partial {R_S}^{n}}{\partial {u_S}^{n}} \end{array}\right] \left[\begin{array}{c} \frac{\partial {u_T}^{n-1}}{\partial D} \\ \frac{\partial {u_S}^{n-1}}{\partial D} \\ \hline \frac{\partial {u_T}^{n}}{\partial D} \\ \frac{\partial {u_S}^{n}}{\partial D} \end{array}\right] = \left[\begin{array}{c} -\frac{\partial {R_T}^{n-1}}{\partial D} \\ -\frac{\partial {R_S}^{n-1}}{\partial D} \\ \hline -\frac{\partial {R_T}^{n}}{\partial D} \\ -\frac{\partial {R_S}^{n}}{\partial D} \end{array}\right] \tag{37}$$

For the simple case of a single design parameter *D*, this forms a block lower triangular linear system where the unknown state variable sensitivities and the right-hand-side form vectors rather than matrices. Thus, the system can be solved using forward substitution, i.e. a forward sweep in time beginning at time step *n - 1*, and progressing to time-step *n*. At each time-step, a fully coupled linear system is solved iteratively to obtain the sensitivity of the state variables at that time step to the single design parameter. For the case of multiple design inputs *D*, the forward sweep in time along with the coupled linear solution at each time-step has to be performed for each parameter in order to construct the state variable sensitivity matrix for each discipline one column at a time. Once the state variable sensitivity matrices are available, they can be substituted into Eq. (22), where the inner product can be evaluated and the complete gradient vector $\frac{dL}{dD}$ becomes available [21, 41, 56, 57].

Following the same derivation as given above for the tangent linearization, again we assume a problem with two disciplines, and two time-steps, *n* and *n-1*. For this case the adjoint system can be discretely expanded in time and expressed as:

$$\left[\begin{array}{cc|cc} \frac{\partial R_T^{n-1}}{\partial u_T^{n-1}}^T & \frac{\partial R_T^{n}}{\partial u_T^{n-1}}^T & \frac{\partial R_S^{n-1}}{\partial u_T^{n-1}}^T & \frac{\partial R_S^{n}}{\partial u_T^{n-1}}^T \\ 0 & \frac{\partial R_T^{n}}{\partial u_T^{n}}^T & 0 & \frac{\partial R_S^{n}}{\partial u_T^{n}}^T \\ \hline \frac{\partial R_T^{n-1}}{\partial u_S^{n-1}}^T & \frac{\partial R_T^{n}}{\partial u_S^{n-1}}^T & \frac{\partial R_S^{n-1}}{\partial u_S^{n-1}}^T & \frac{\partial R_S^{n}}{\partial u_S^{n-1}}^T \\ 0 & \frac{\partial R_T^{n}}{\partial u_S^{n}}^T & 0 & \frac{\partial R_S^{n}}{\partial u_S^{n}}^T \end{array}\right] \left[\begin{array}{c} \Lambda_T^{n-1} \\ \Lambda_T^{n} \\ \hline \Lambda_S^{n-1} \\ \Lambda_S^{n} \end{array}\right] = \left[\begin{array}{c} \frac{\partial L}{\partial u_T^{n-1}}^T \\ \frac{\partial L}{\partial u_T^{n}}^T \\ \hline \frac{\partial L}{\partial u_S^{n-1}}^T \\ \frac{\partial L}{\partial u_S^{n}}^T \end{array}\right] \tag{38}$$

Which can be rearranged into a block upper triangular form as shown below:

$$\left[\begin{array}{cc|cc} \frac{\partial R_T^{n-1}}{\partial u_T^{n-1}}^T & \frac{\partial R_S^{n-1}}{\partial u_T^{n-1}}^T & \frac{\partial R_T^{n}}{\partial u_T^{n-1}}^T & \frac{\partial R_S^{n}}{\partial u_T^{n-1}}^T \\ 0 & \frac{\partial R_S^{n-1}}{\partial u_S^{n-1}}^T & 0 & \frac{\partial R_S^{n}}{\partial u_S^{n-1}}^T \\ \hline 0 & 0 & \frac{\partial R_T^{n}}{\partial u_T^{n}}^T & \frac{\partial R_S^{n}}{\partial u_T^{n}}^T \\ 0 & 0 & 0 & \frac{\partial R_S^{n}}{\partial u_S^{n}}^T \end{array}\right] \left[\begin{array}{c} \Lambda_T^{n-1} \\ \Lambda_S^{n-1} \\ \hline \Lambda_T^{n} \\ \Lambda_S^{n} \end{array}\right] = \left[\begin{array}{c} \frac{\partial L}{\partial u_T^{n-1}}^T \\ \frac{\partial L}{\partial u_S^{n-1}}^T \\ \hline \frac{\partial L}{\partial u_T^{n}}^T \\ \frac{\partial L}{\partial u_S^{n}}^T \end{array}\right] \tag{39}$$

This system can be solved through back substitution, i.e. a backward sweep in time, where a coupled linear system is solved at time step *n* before progressing backward to time step *n - 1*. At each time step a coupled iterative linear solution is required in order to determine the vector of unknown disciplinary adjoint variables at that time step. Once the vector of disciplinary adjoint variables spanning the spatial and temporal domains is available, it may be substituted into the total sensitivity equation shown in Eq. (34). Again, the effect of the number of design inputs *D* has been confined to a series of matrix-vector products at the end of the computation. The elegance of the method lies in the fact that only a single backward sweep in time with coupled linear solutions at each time step is required in order to compute the total gradient, contrary to the tangent linearization. The determination of the gradient vector therefore involves a single forward integration in time to obtain the solution to the coupled unsteady analysis problem, and a single backward sweep in time to obtain the necessary adjoint variables [21, 41, 56, 57]. In AStrO, the transient thermo-elastic analysis is performed first and the solution at every time step is written to disk. Later, in the adjoint calculation, this solution at each time step is read back in during the backward sweep in time.

C. Verification of the Sensitivities

In this study we have verified the tangent and adjoint sensitivities for the coupled thermo-elastic problems using the complex-step method. This method is very similar to the finite-difference. However, in this case the perturbation is introduced to the imaginary part of the input. This is demonstrated more clearly in the Taylor series expansion below [18, 58]:

$$f(x+ih) = f(x) + ihf'(x) - \frac{h^2}{2}f''(x) + \cdots \tag{40}$$

From which the derivative $f'(x)$ can be easily determined as:

$$f'(x) = \frac{Im[f(x+ih)]}{h} \tag{41}$$

As seen above, similar to the finite-difference method, the complex-step method also requires a step size. However, the complex-step method is not sensitive to the step size selection. This is because no differencing is required, which results in the high accuracy of the derivatives. In theory, it is possible to verify tangent and adjoint-based gradients using the complex-step method to machine precision. With this in mind, a complex version of AStrO has been constructed. The main disadvantage of the complex-step method is the large increase in the runtime

required when using complex arguments [18, 58]. Therefore, in this study the sensitivities calculated by the complex-step method are only used for verification purposes and not for the actual optimization process.

V. Thermo-Elastic Sensitivity Analysis Validation for the Structural Solver

AStrO has been validated by performing unit tests on each element type and comparing results either with analytical solutions when available, or with solutions generated by Abaqus [29, 41]. The elastic and aero-elastic analysis and sensitivity calculation capabilities of AStrO had been demonstrated in previous work [14, 29, 34, 35, 41]. In reference [22] we presented results for the validation of AStrO's heat conduction solution capability as well as the thermo-elastic analysis capability.

In this section validation results for the thermo-elastic sensitivity analysis and optimization capabilities of AStrO are presented. In the following we first present results for the validation of static thermo-elastic sensitivity analysis with both the tangent and adjoint methods in AStrO for two cases: a rectangular bar with applied elastic and thermal loads, and a heated panel case. Next, we move on to presenting results for a transient thermo-elastic sensitivity analysis. For each case mentioned the adjoint linearization is verified using the duality relation [44] to the tangent approach, while the tangent sensitivities are verified with the complex-step method [34, 58]. Also, for all the optimization cases presented in the coming pages, AStrO's internal optimizer has been used. As mentioned before, this on-board optimizer uses the steepest-descent line search algorithm with backtracking [44].

A. Static Thermo-Elastic Sensitivity Analysis and Optimization Validation for a Rectangular Bar with Applied Elastic and Thermal Loads

For this first case we study the thermo-elastic sensitivity analysis and optimization in a rectangular bar with both thermal and elastic loads applied. The bar has a length of $10m$ in the z-direction, and $1m$ in both the x- and y-direction. The mesh used for this study has 44 nodes and 10 hexahedral elements.

The applied boundary conditions are summarized in Fig. 4. The corners of the lower x-face are fixed to zero displacement and a temperature of zero degrees Celsius is applied at these corners. A constant heat flux of 7 W/m^2 is applied to the upper x-face of the bar. Also, a positive force of $1N$ is applied to the points at the center of the bar on the top x-face in the negative x-direction. The material properties of the rectangular bar are presented in Table 1.

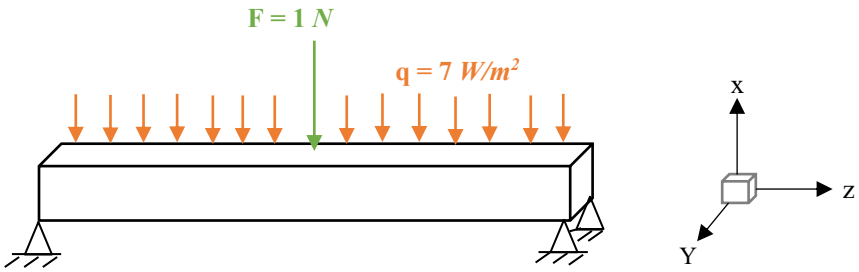

Fig. 4 Applied boundary conditions for the thermo-elastic sensitivity calculation and optimization of the rectangular bar case.

Table 1 Rectangular bar material properties.

Property	*Value*
Thermal Conductivity *(k)*	1.0 *W/(m.K)*
Thermal expansion (α)	10^{-4} *1/K*
Modulus of elasticity (E)	10^6 *N/m²*
Poisson's ration (ν)	0.3 (dimensionless)

1) *Sensitivity Analysis Validation for the Rectangular Bar Case*

For this case we are defining the objective function to be the square of the displacement at the center of the bar in the x-direction. The objective function for this case is defined as:

$$L = (Displacement\_X(i))^2 \tag{42}$$

where ‘i’ is the index of the center node on the bottom x-face of the bar.

To test the adjoint-based sensitivities, the elastic modulus, thermal conductivity and coefficient of thermal expansion of the rectangular bar are defined as the design variables. The sensitivity of each property was scaled to the original value, resulting in the following design-dependent definitions:

$$\begin{cases} E = E_0 + 10^6 D_1 \\ k = k_0 + D_2 \\ \alpha = \alpha_0 + 10^{-4} D_3 \end{cases} \tag{43}$$

The adjoint and tangent formulations are mathematically equivalent, using exact differentiation of the governing equations, and they agree nearly to machine precision. Complex differentiation does not use the linearization of the governing equations but works much like a high-precision finite-difference and is also numerically equal to the other two results. The presented sensitivities in Table 2 indicate that the adjoint implementation correctly differentiates the finite element solution in this case.

Table 2: Comparison of the objective function sensitivities for the rectangular bar case with applied thermal and structural loads (objective is a function of the displacement in the x-direction at the center of the bar).

	Adjoint	***Tangent***	***Complex***
D_1 −Modulus of elasticity (E)	- 0.0002479963569	- 0.0002479963569	- 0.0002479963569
D_2 −Thermal Conductivity *(k)*	- 0.2890102246446	- 0.2890102246446	- 0.2890102246446
D_3 −Thermal expansion (α)	0.5857706751382	0.5857706751382	0.5857706751382

2) Thermo-Elastic Optimization for the Rectangular Bar Case

After the sensitivities calculated using the adjoint-based method were verified, we used these sensitivities to do a thermo-elastic optimization study on the rectangular bar using AStrO. The goal in this optimization problem is to minimize the objective function presented in Eq. (42) with respect to the design variables defined in Eq. (43). The vector of design variable contains both elastic and thermal material properties. The objective function, which is created from the deformation of the rectangular bar in the x-direction, is a function of both thermal and elastic material properties.

Table 3 shows the change in the objective function from the baseline rectangular bar to the thermo-elastically optimized case. The initial and optimized material properties are summarized in Table 4. These changes in the material properties allow the thermal deflection to balance the applied force. Contours of the displacement in the x-direction for the baseline and thermo-elastically optimized rectangular bar are shown in Fig. 5 and Fig. 6 respectively. It can be seen from the results in Table 3, Fig. 5 and Fig. 6 that the displacement in the x-direction at the bottom center of the bar is now zero. The convergence of the optimization process for the rectangular bar case is shown in Fig. 7. After 11 optimization cycles the optimizer was able to find the optimum solution.

Table 3: Comparison of the change in the objective function for the baseline and thermo-elastically optimized rectangular bar.

	Baseline	***Thermo-elastic optimization***
Objective Function (Eq. (42))	0.14439066575919221	$1.0132638884907125\times10^{-10}$

Table 4: Initial and optimized material properties of the static rectangular bar case after the thermo-elastic optimization process.

Material Properties	***Initial Material Properties***	***Optimized Material Properties***
Modulus of elasticity (E)	10^6 *N/m²*	1.000042931×10^6 *N/m²*
Thermal Conductivity (k)	1.0 *W/(m.K)*	1.13765820913759477*W/(m.K)*
Thermal expansion (α)	10^{-4} *1/K*	0.50708×10^{-6} *1/C*

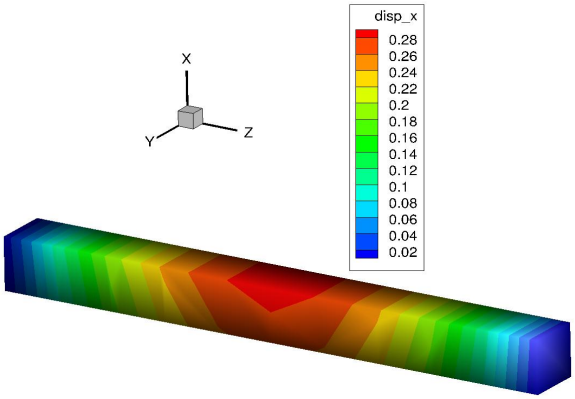

Fig. 5 Displacement of the rectangular bar in the x-direction for the baseline case.

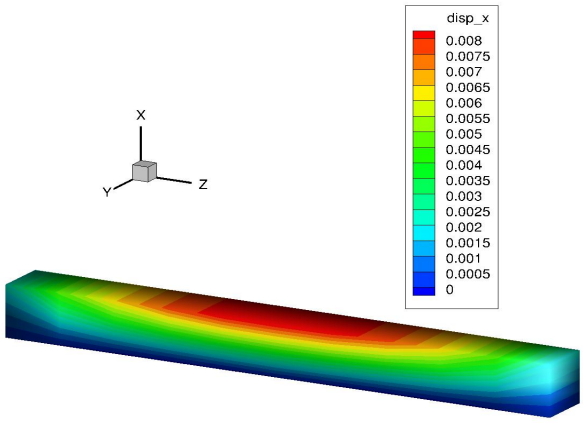

Fig. 6 Displacement of the rectangular bar in the x-direction after thermo-elastic optimization.

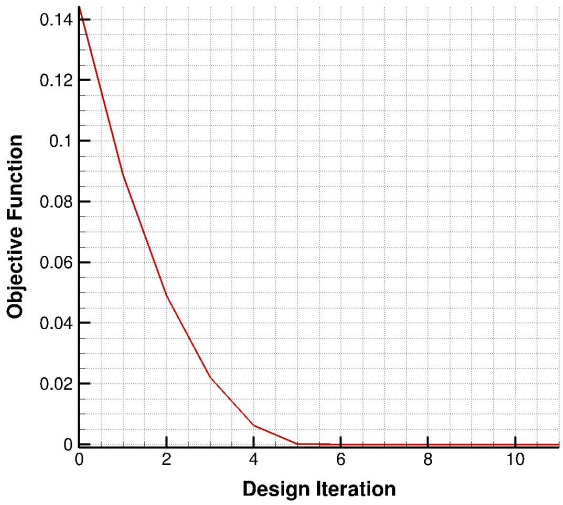

Fig. 7 Convergence of the thermo-elastic optimization process for the rectangular bar case with applied thermal and elastic load.

B. Static Thermo-Elastic Sensitivity and Optimization Study of a Heated Panel Case

As mentioned previously, the fluid/thermal/structural interactions play an important role in many design problems. One such problem is the thermal protection systems on hypersonic flight vehicles. The study of aerodynamically heated panels is a preliminary but important step towards the objectives of analyzing more realistic material and structures for such vehicles [59]. For this reason, in the next two validation cases we study the sensitivity analysis and optimization process of heated panel cases.

As shown in Fig. 8 the panel for this first case is made of multiple layers of material. The test panel is 4*in* long, has a thickness of 0.1*in*, and a width of 0.5*in.* The panel mesh 5,628 nodes and 3,990 hexahedral elements. The description of the material properties of the panel is summarized in Table 5. As can be seen there are three layers of material in this panel, the top layer, which acts as the thermal protection layer on the panel and is made of Inconel 718, the middle layer, which is the insulation layer, is made of Saffil, and the bottom layer, which is made of AL 2024. The thickness of each layer of material is the same and equal to 0.33333 *in*.

Table 5 Description of the material property of the different layers of the static heated panel case [60].

Property	***Thermal Protection layer (Top layer)***	***Insulation layer (Middle layer)***	***Bottom layer***
Material	**Inconel 718**	**Saffil**	**Al 2024**
Density *(ρ)*	0.29443743 lbm/in^3	0.001806365 lbm/in^3	0.09284714 lbm/in^3
Thermal Conductivity *(k)*	0.140442×10^{-3} *BTU/(s.in.R)*	0.00104329×10^{-3} *BTU/(s.in.R)*	1.070037×10^{-3} *BTU/(s.in.R)*
Specific heat capacity *(C)*	0.097926818 *BTU/(lbm.R)*	0.224992835 *BTU/(lbm.R)*	0.225470526 *BTU/(lbm.R)*
Thermal expansion (α)	5.83333×10^{-6} *1/R*	1×10^{-10} *1/R*	8.88889×10^{-6} *1/R*
Modulus of elasticity (E)	2.8282183×10^{7} lbf/in^2	4.351105181×10^{4} lbf/in^2	9.862505076×10^{6} lbf/in^2
Poisson's ration (v)	0.28 (dimensionless)	0.26 (dimensionless)	0.32 (dimensionless)

The panel is supported by immovable supports on the left and right edges of the bottom surface. The bottom surface of the panel is insulated, while the faces on the right and left side of the panel have a constant temperature equal to the initial temperature of 530R. A uniform heat flux of 0.02 $\frac{BTU}{in^2.s}$ is applied to the top surface of the panel. This thermal boundary condition is applied in order to mimic the aerodynamic heating of the panel for the thermo-elastic optimization. Under these thermal and structural boundary conditions, the panel deforms into a convex shape as shown in Fig. 9.

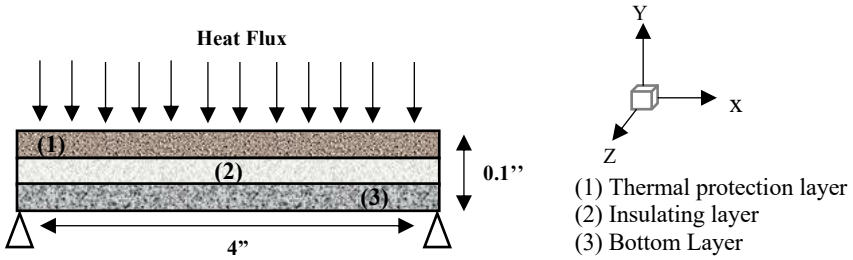

Fig. 8 Coupled thermal/structural model and boundary conditions for the static heated panel made of multiple materials.

Fig. 9 Panel with convex deformation.

1) Sensitivity Analysis Validation for the Static Heated Panel Case

For this case the objective function is defined to keep the average temperature of the bottom layer of the panel as close as possible to $T_{limit} = 930R$, which is much lower than the value obtained from the baseline panel design, as can be seen later from the results. This objective function is chosen because the convex deformation of the panel is a direct result of the rise in the temperature of the panel. Hence, the objective function for this case is defined as:

$$L = \left(\sum_{i=1}^{n} \frac{(Temperature(i) - T_{limit})^2}{n^2}\right) + 10^5 \times (Mass_{top\ layer} - 2.5 \times Mass_{inital\ top\ layer})^2 \quad (44)$$

where 'i' is the node number and 'n' is the total number of nodes that make up the mesh for the bottom layer of the panel. Also, please note that in Eq. (44) a mass penalty is used. This is because the thickness of the top layer is used as a design variable in this problem.

To test the adjoint-based sensitivities, the elastic modulus, thermal conductivity, coefficient of thermal expansion of the thermal protection layer (top layer), and the thickness of the top layer of the panel are defined as the design variables. The sensitivity of each property was scaled to the original value, resulting in the following design-dependent definitions:

$$\begin{cases} E_{Top\ layer} = E_0 + 2 \times 10^6 D_1 \\ k_{Top\ layer} = k_0 + 10^{-3} D_2 \\ \alpha_{Top\ layer} = \alpha_0 + 5 \times 10^{-5} D_3 \\ Thickness_{Top\ layer} = Thickness_{intial-top\ layer} \times D_4 \end{cases} \quad (45)$$

The adjoint based sensitivities were verified against the sensitivities calculated by the tangent and complex-step method. The results are shown in Table 6. As can be seen the sensitivity of the objective function with respect to the modulus of elasticity and thermal expansion is zero. Since the objective function is based on temperature, this is to be expected because of the one-way dependence of deformation on temperature in AStrO. The sensitivity of the objective function with respect to the thermal conductivity and thickness, match for the adjoint, tangent and complex differentiation, up to machine precision.

Table 6: Comparison of the objective function sensitivities for the static heated panel case for the adjoint, tangent and complex-step methods.

	Adjoint	***Tangent***	***Complex***
D_1 −Modulus of elasticity (E)	0.000000000000	0.000000000000	0.000000000000
D_2 −Thermal Conductivity *(k)*	-215.2563863794**097**	-215.2563863794**0875**	-215.2563863794**592**
D_3 −Thermal expansion (α)	0.000000000000	0.000000000000	0.000000000000
$D_4 - Thickness$	-145.826189500**7903**	-145.826189500**7905**	-145.826189500**8018**

2) Thermo-Elastic Optimization for the Static Heated Panel Case

After the sensitivities calculated using the adjoint-based method were verified, we used these sensitivities to run a thermo-elastic optimization process for this static multi-layered panel case using AStrO. The goal in this optimization problem is to minimize the objective function presented in Eq. (44) with respect to the thermal conductivity and the thickness of the thermal protection layer, which forms the top layer of the panel. Table 7 shows the change in the objective function from the baseline panel to the thermo-elastically optimized panel case. Contours of the temperature for the baseline and thermo-elastically optimized panel are shown in Fig. 10. From these results it is obvious that the average temperature of the lower part of the panel has decreases as was desired.

Table 7: Comparison of the baseline and thermo-elastically optimized objective function for the static panel case.

	Baseline	***Thermo-elastic optimization***
Objective function (Eq. (44))	137.10305736304662	12.496144040068716

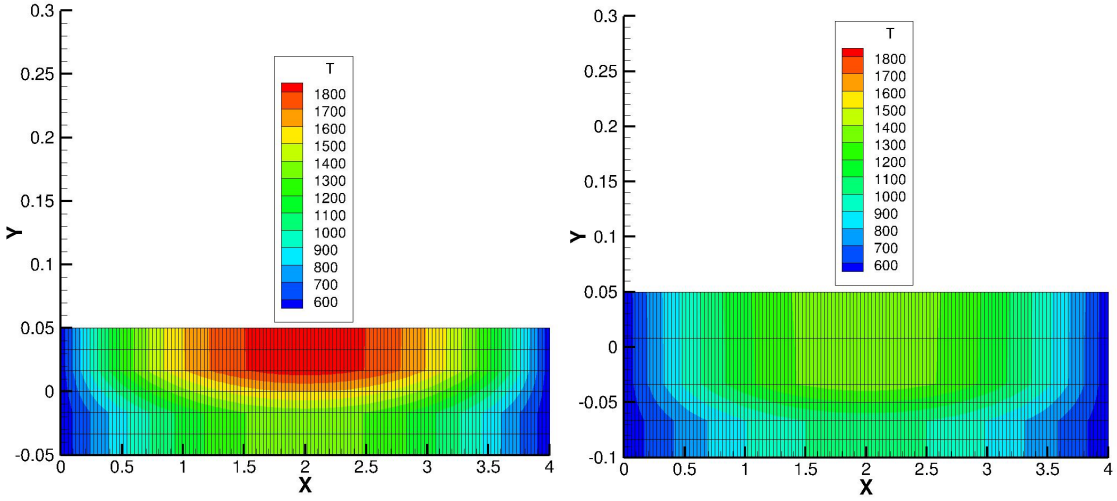

Fig. 10 Temperature for both the baseline (on the left) and the thermo-elastically optimized (on the right) for the static heated panel case.

The initial and optimized material properties of the panel are summarized in Table 8 below. It can also be seen that the thickness of the top layer has increased but in a constrained manner due to the penalty put on the mass. The increase in the thermal conductivity of the top layer is less expected. However, that is explained by the boundary conditions of this problem. A Dirichlet boundary condition of 530*R* is applied to the two sides of the panel. The convergence of the optimization process for the static heated panel case is shown in Fig. 11, where the objective is seen to be reduced by a factor of 11 over 13 design steps.

Table 8: Changes in the design variables and optimized material properties of the static heated panel case.

Material Properties of the top layer	***Initial Material Properties***	***Optimized Material Properties***
Thermal Conductivity (k)	0.140442×10^{-3} *BTU/(s.in.R)*	0.3133×10^{-3} *BTU/(s.in.R)*
Thickness	0.0333333 *in*	0.08325182 *in*

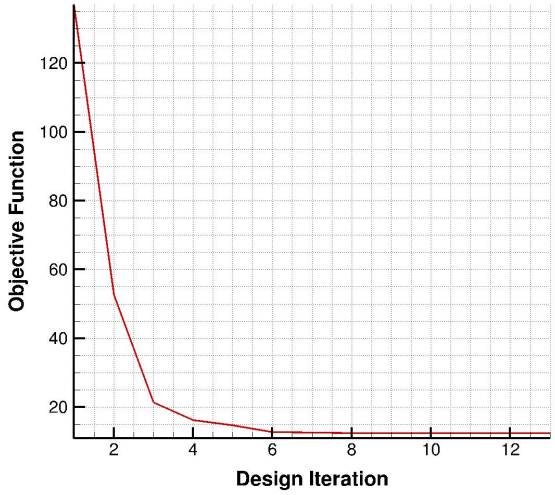

Fig. 11 Convergence of the thermo-elastic optimization process for the static heated panel case.

C. **Transient Thermo-Elastic Sensitivity Analysis of a Heated Panel Case**

In this section the sensitivities calculated using the discrete adjoint method, for a transient thermo-elastic problem of an aerodynamically heated panel case, are validated. We consider the case of a thin panel subjected to aerodynamic heating. This test case was first studied in reference [61]. In reference [22] we used the same case to validate AStrO's thermo-elastic analysis capabilities, and the aero-thermo-elastic analysis platform developed in-house.

1) Description of Thermo-Elastic Computational Set-Up for the Transient Heated Panel Case

A schematic of the computational model and boundary conditions for this problem is shown in Fig. 12. The panel is supported by immovable supports on the left and right edges of the bottom surface. The bottom surface of the panel is insulated, while the faces on the right and left side of the panel have a constant temperature equal to the initial temperature of 530*R*. A uniform heat flux is applied to the top surface of the panel. Under these thermal and structural boundary conditions, the panel deforms into a convex shape [59, 61, 62].

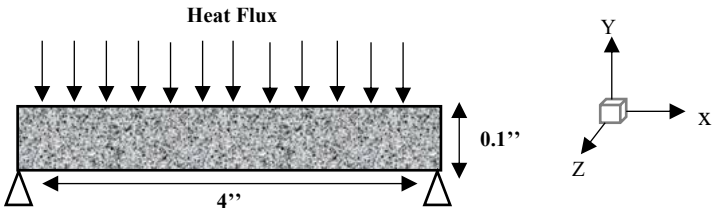

Fig. 12 Coupled thermal/structural model and boundary conditions for the transient heated panel case.

The test panel is 4*in* long, has a thickness of 0.1*in*, and a width of 0.5*in.* It is made from AM-350 stainless steel. The properties of the panel are tabulated in Table 9 [62].

Table 9 Transient heated panel material properties [62].

Property	***Value***
Density *(ρ)*	0.282 lbm/in^3
Thermal Conductivity *(k)*	0.12864×10^{-3} *BTU/(s.in.R)*
Specific heat capacity *(C)*	0.11162 *BTU/(lbm.R)*
Thermal expansion (*α*)	0.62643×10^{-5} *1/R*
Modulus of elasticity (*E*)	0.35346×10^{8} lbf/in^2
Poisson's ration (*v*)	0.25 (dimensionless)

At these early times, the heating rate across the panel is nearly uniform, and can be approximated by the following equation [62]:

$$\dot{q}(t) = 0.026 - 0.0001t \ (\frac{BTU}{in^2.s}) \tag{46}$$

Equation (46) is used as a thermal boundary condition in order to mimic the aerodynamic heating for the thermo-elastic problem. The time step used for the coupled thermo-elastic analysis was 1*s*. Hence 30 time-steps were required to heat the panel for 30*s.*

2) Thermo-Elastic Sensitivity Analysis Validation for the Transient Panel Case

For this case the objective function is derived using the deformation of the panel in the x- and y-directions, as shown below:

$$L = \sum_{i=1}^{n} (Disp\_x(i))^2 + (Disp\_y(i))^2 \tag{47}$$

where 'i' is the node number and 'n' is the total number of nodes in the panel. The mesh used in this study has 3,216 nodes, and 1,995 hexahedral elements.

To test the adjoint-based sensitivities, the elastic modulus, thermal conductivity, coefficient of thermal expansion, and the specific heat capacity of the panel material were defined as the design variables. The sensitivity of each property was scaled to the original value, resulting in the following design-dependent definitions:

$$\begin{cases} E = E_0 + 10^7\, D_1 \\ k = k_0 + 10^{-4} D_{\,2} \\ \alpha = \alpha_0 + 10^{-6} D_3 \\ C = C_0 + 10^{-1} D_4 \end{cases} \tag{48}$$

The adjoint-based sensitivities were verified against the sensitivities calculated by the tangent and complex-step method. Table 10-13 compare the coupled thermo-elastic sensitivities obtained from the complex analysis run with those of the tangent and adjoint linearization for 6 different time steps. Each table presents the results for one of the design variables defined in Eq. (48). As shown in these tables, the sensitivity values from the tangent and adjoint linearization matches up to machine precision with the complex-step method.

Table 10: Comparison of the objective sensitivities for the transient heated panel case for the adjoint, tangent and complex-step methods for design variable D_1 as defined in Eq. (48).

Time step	*Adjoint*	*Tangent*	*Complex*
5	-0.000565874550**9**	-0.000565874550**9**	-0.000565874551**0**
10	-0.004184719199**2**	-0.004184719199**2**	-0.004184719199**6**
15	-0.013242515647**3**	-0.013242515647**2**	-0.013242515648**4**
20	-0.029733737043**2**	-0.029733737043**2**	-0.029733737045**8**
25	-0.055351855920**3**	-0.055351855920**3**	-0.055351855924**9**
30	-0.091535337207**0**	-0.091535337207**1**	-0.091535337214**7**

Table 11: Comparison of the objective sensitivities for the transient heated panel case for the adjoint, tangent and complex-step methods for design variable D_2 as defined in Eq. (48).

Time step	*Adjoint*	*Tangent*	*Complex*
5	-0.0270281059525	-0.0270281059525	-0.0270281059525
10	-0.142442720857**7**	-0.142442720857**7**	-0.142442720857**8**
15	-0.423507682146**4**	-0.423507682146**2**	-0.423507682146**5**
20	-0.963703387967**1**	-0.963703387967**3**	-0.963703387967**5**
25	-1.865630899433**7**	-1.865630899433**6**	-1.865630899433**9**
30	-3.237266177716**8**	-3.237266177717**8**	-3.237266177718**4**

Table 12: Comparison of the objective sensitivities for the transient heated panel case for the adjoint, tangent and complex-step methods for design variable D_3 as defined in Eq. (48).

Time step	*Adjoint*	*Tangent*	*Complex*
5	0.0644539160860	0.0644539160860	0.0644539160860
10	0.421461716355**5**	0.421461716355**6**	0.421461716355**7**
15	1.288937496192**9**	1.288937496192**4**	1.288937496192**9**
20	2.852209288536**0**	2.852209288535**4**	2.852209288536**7**
25	5.269683857648**1**	5.269683857645**9**	5.269683857648**1**
30	8.676460311079**9**	8.676460311079**7**	8.676460311083**4**

Table 13: Comparison of the objective sensitivities for the transient heated panel case for the adjoint, tangent and complex-step methods for design variable D_4 as defined in Eq. (48).

Time step	*Adjoint*	*Tangent*	*Complex*
5	-0.329838517524**0**	-0.329838517524**3**	-0.329838517524**4**
10	-2.196336765060**2**	-2.196336765060**2**	-2.196336765061**5**
15	-6.732099087170**7**	-6.732099087168**2**	-6.732099087170**7**
20	-14.868779182942**0**	-14.868779182939**4**	-14.868779182946**1**
25	-27.376707081780**6**	-27.376707081773**3**	-27.376707081781**6**
30	-44.889379863616**3**	-44.889379863614**6**	-44.889379863635**5**

VI. Thermo-Elastic Optimization for Aero-thermo-elastic Problems

In this section, we look at the aero-thermo-elastic analysis solution for a transient aerodynamically heated panel case. We will compare the aero-thermo-elastic solution for a baseline panel design with the thermo-elastically optimized panel. This is done to show how the thermo-elastic optimization of the panel changes the flow solution.

A. Thermo-Elastic Design Optimization for the Transient Aerodynamically Heated Panel Case

The panel used for this optimization study has the same material properties as the transient heated panel case presented in the previous section. These material properties are summarized in Table 9. A schematic of the computational model and boundary conditions for this problem is shown in Fig. 13. The panel is supported by immovable supports on the left and right edges of the bottom surface. The bottom surface of the panel is insulated, while the faces on the right and left side of the panel have a constant temperature equal to the initial temperature of $530R$. A uniform heat flux and a uniform aerodynamic force are applied to the top surface of the panel.

The applied uniform heat flux and aerodynamic boundary conditions are intended to mimic the aerodynamic heating and forces for the thermo-elastic problem. The aerodynamic force across the panel is nearly uniform and has a value of $0.002N$. The heating rate across the panel is nearly uniform, and can again be approximated by Eq. (46) presented in the previous section [62].

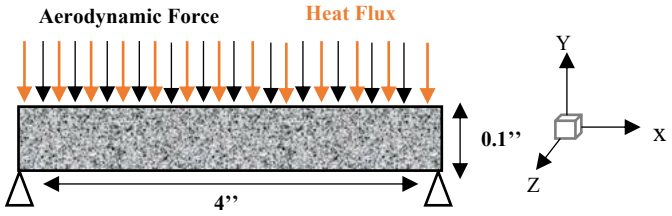

Fig. 13 Coupled thermal/structural model and boundary conditions for the transient aerodynamically heated panel case.

The goal in this optimization problem is to minimize the objective function presented in Eq. (47) with respect to the design variables defined by Eq. (48). The vector of design variable contains both elastic and thermal material properties. The objective function, which is created from the deformation of the panel in the x- and y-direction, is a function of both thermal and elastic material properties. To make sure that realistic material properties are obtained after the optimization process, the design variables were bounded as follows:

$$\begin{cases} -0.188 \le D_1 \le 0.188 \\ -0.72 \le D_2 \le 0.72 \\ -2.0 \le D_3 \le 2.0 \\ -0.1 \le D_4 \le 0.1 \end{cases} \tag{49}$$

The time step used for the coupled thermo-elastic analysis was $1s$. Hence 30 time-steps were required to heat the panel for $30s$. Table 14 shows the change in the objective function from the baseline panel to the thermo-elastically optimized panel case. Contours of the displacement in the x- and y-directions for the baseline and thermo-elastically optimized panel are shown in Fig. 14 and Fig. 15. From these results, it is clear that the convex deformation of the panel is drastically reduced due to the optimization process.

Table 14: Comparison of the baseline and thermo-elastically optimized objective function for the transient aerodynamically heated panel case.

	Baseline	***Thermo-elastic optimization***
Objective function (Eq. (62))	25.78179928166821	9.37336380561037

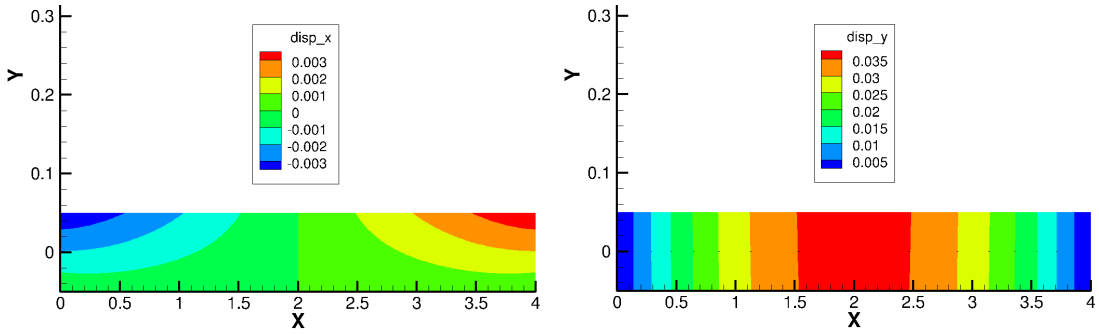

Fig. 14 Contours of displacement in the x- and y- direction for the baseline transient aerodynamically heated panel case as calculated by AStrO.

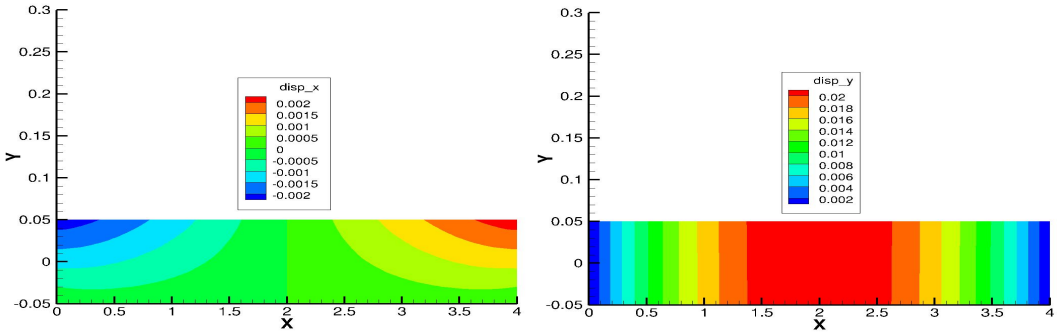

Fig. 15 Contours of displacement in the x- and y- direction for the thermo-elastically optimized transient aerodynamically heated panel case as calculated by AStrO.

In order to achieve the minimum displacement in the x- and y-direction for this panel under the specified boundary conditions applied, the material properties of the panel would have to change. The changes in the design variables, which reflect the changes in the material properties of the panel, are summarized in Table 15 below.

Table 15: Changes in the design variables and optimized material properties of the transient aerodynamically heated panel case after the thermo-elastic optimization process.

Changes in Design Variable		***Optimized Material Properties***	
D_1	-0.0187990804614502	***Modulus of elasticity (E)***	0.35180092 $\times 10^{8}$ *lbf/in*^{2}
D_2	0.71999921174524073	***Thermal Conductivity (k)***	0.200639 $\times 10^{-3}$ *BTU/(s.in.R)*
D_3	-1.9999603748447023	***Thermal expansion (α)***	4.26433 $\times 10^{-6}$ *1/R*
D_4	0.09991144164202264	***Specific heat capacity (C)***	0.1216111*BTU/(lbm.R)*

The convergence of the optimization process for the panel case is shown in Fig. 16. After 159 optimization cycles the process is terminated due to the bounds put on the design variables.

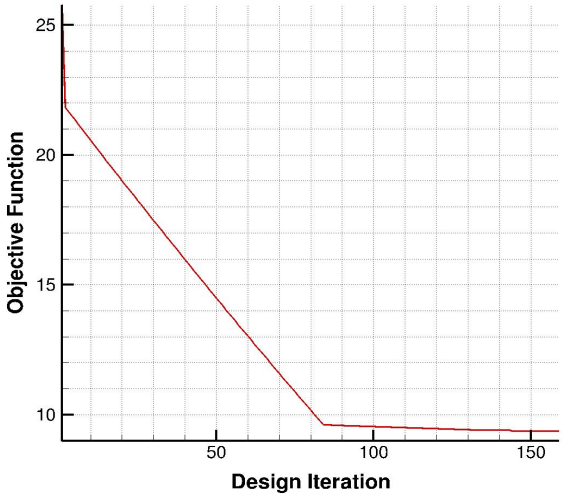

Fig. 16 Convergence of the thermo-elastic optimization process for the transient aerodynamically heated panel case.

B. Description of the Aero-Thermo-Elastic Computational Set-Up for the Transient Aerodynamically Heated Panel Case

A schematic of the experiment that can be used to validate the flow/thermal/structural analysis of this problem as presented in reference [62] is shown in Fig. 17 below. In reference [22] we validated our developed aero-thermo-elastic platform for this specific case.

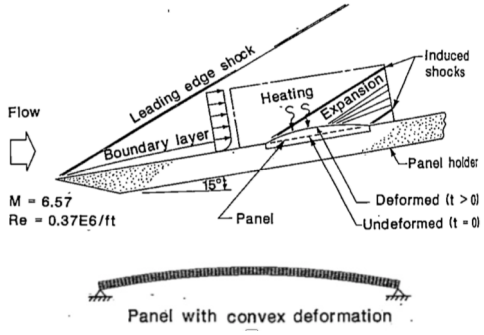

Fig. 17 Schematic diagram of the experiment that can be used to validate the flow/thermal/structural analysis of the aerodynamically heated panel case reproduced from reference [62].

The fluid mesh used for this study has 2,474,940 nodes, with 4,725,000 prism elements. The fluid mesh has a wall spacing of 6×10^{-6}, which gives a Y^{+} of less than one along the panel surface. The structure mesh used in this coupled simulation has 3,216 nodes, with 1,995 hexahedral elements.

The boundary conditions applied to the coupled problem are summarized in Fig. 18. The top surface of the panel, which is the fluid/structure interface, has a surface heat flux applied on the structure side, and an applied temperature enforced from the structure side on to the fluid side. The sides of the panel are considered isothermal, with an applied temperature of 530*R.* The panel is fixed on the left and right edges of the bottom surface. The initial free-stream flow parameters for this case are described in Table 16.

Since the flow field reaches equilibrium much faster than the thermal response of the panel structure, the coupled problem is solved as a steady-state problem on the fluid side and as a transient problem on the structural side. The time step for the thermal solver is taken as 5s. Thus, it takes six coupled cycles between the fluid and structure solvers to reach the transient solution at thirty seconds.

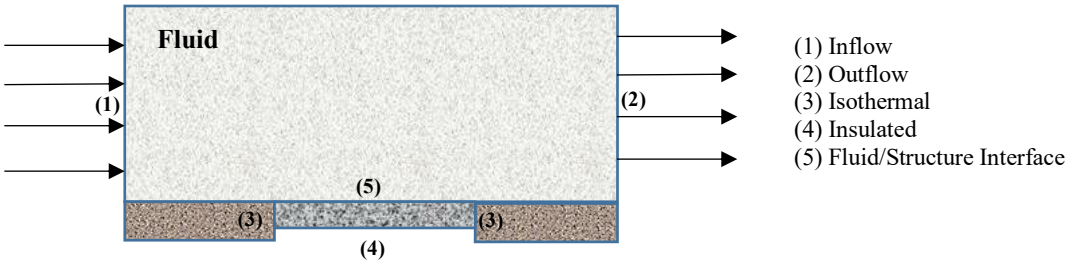

Fig. 18 Applied boundary conditions for the aero-thermo-elastic problem of the transient aerodynamically heated panel case.

Table 16 Initial free-stream conditions for the coupled flow over the transient aerodynamically heated panel.

Free-stream conditions	***Value***
Free-stream Mach number (Ma_∞)	6.57 (dimensionless)
Wall temperature (T_w)	530 K
Free-stream Reynolds number (Re_∞)	0.66×10^6 $1/ft$
Free-stream temperature (T_∞)	530 K
Free-stream velocity (U_∞)	6612.3 ft/s
Free-stream pressure (P_∞)	0.0971 psi

In the following, aero-thermo-elastic analysis for the baseline panel design and the optimized panel design from AStrO's thermo-elastic optimization is presented. The meshes for both cases are the same. The difference between the two cases is the material properties of the panels. The material properties of the two panel cases are summarized in Table 17 below.

Table 17 Material properties for the baseline and thermo-elastically optimized transient aerodynamically panel cases.

Property	***Baseline Panel Design***	***Thermo-Elastically Optimized Panel Design***
Density (ρ)	0.282 lbm/in^3	0.282 lbm/in^3
Thermal Conductivity (k)	0.12864×10^{-3} $BTU/(s.in.R)$	0.200639×10^{-3} $BTU/(s.in.R)$
Specific heat capacity (C)	0.11162 $BTU/(lbm.R)$	$0.1216111 BTU/(lbm.R)$
Thermal expansion (α)	0.62643×10^{-5} $1/R$	4.26433×10^{-6} $1/R$
Modulus of elasticity (E)	0.35346×10^8 lbf/in^2	0.35180092×10^8 lbf/in^2
Poisson's ration (v)	0.25 (dimensionless)	0.25 (dimensionless)

C. Numerical Results for the Aero-Thermo-Elastic Analysis of the Baseline and Thermo-Elastically Optimized Transient Aerodynamically Heated Panel Case

In this part numerical results from the aero-thermo-elastic analysis of both the baseline panel design and the thermo-elastically optimized panel design are presented. The interaction between the panel deformation and the flow density distributions at t = 30s for the baseline panel design, and the thermo-elastically optimized panel design, are shown in Fig. 19 and Fig. 20, respectively. In these figures the computed values of density are non-dimensionalised by the free-stream density. Both figures clearly show the development of a shock originating from the left support on the windward side. However, a stronger shock is seen for the baseline panel design. The density of the fluid increases through this shock at first but then decreases as the flow expands over the convex panel. This increase in density is more aggressive in the baseline design than the thermo-elastically optimized panel. The difference between the flow solution in these cases stem from the difference in the deformation of the panel. The maximum deformation for both panels is tabulated in Table 18. A recompression shock is developed as the deformed panel near the right side in both cases turns the flow.

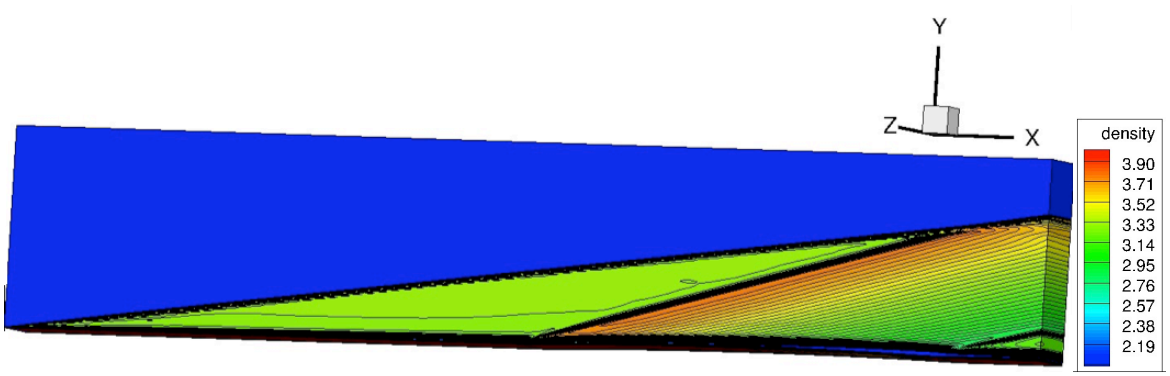

Fig. 19 Flow density distributions at t = 30*s* for the baseline panel design.

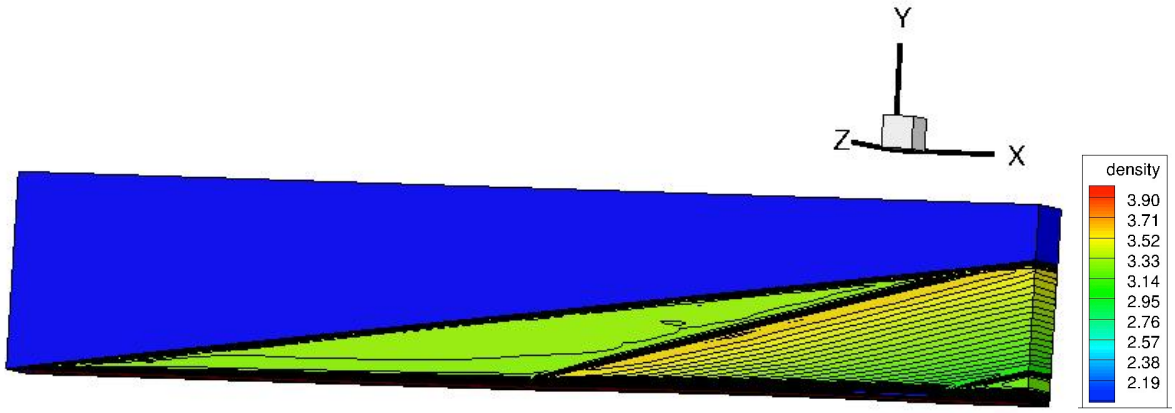

Fig. 20 Flow density distributions at t = 30*s* for the thermo-elastically optimized panel design.

Table 18 Transient Panel case deformation *v (l/2, t)* in inches.

Time(s)	*Coupled computational solution for the baseline panel design*	*Coupled computational solution for the thermo-elastically optimized panel design*
30	0.0369	0.0219

VII. Conclusion

The thermo-elastic sensitivity analysis and optimization capability of AStrO has been validated in this work through multiple examples. In this work we have shown that AStrO has the capability to calculate sensitivities using both the adjoint and tangent method for static and transient coupled thermo-elastic problems. Moreover, an optimized design obtained for a transient thermo-elastic aerodynamically heated panel case was used in an aero-thermo-elastic analysis study using the analysis platform previously developed in-house. This was done to show how the thermo-elastic optimization affects the flow solution. In the future, we hope to be able to further develop our in-house solvers in order to perform coupled aero-thermo-elastic sensitivity analysis and optimization using the discrete adjoint method.

Acknowledgments

This work is supported by ONR Grant N00014-17-1-2337. We are grateful for computer time provided by the NCAR-Wyoming Supercomputer Center (NWSC) and by the University of Wyoming Advanced Research Computing Center (ARCC).

References

[1] Jameson, A., Martinelli, L., and Pierce, N. A. "Optimum aerodynamic design using the Navier-Stokes equations," *Theoretical and Computational Fluid Dynamics* Vol. 10, No. 1-4, 1998, pp. 213-237. doi: 10.1007/s001620050060

[2] Witherden, F., D.;Jameson,A. "Future Directions of Computational Fluid Dynamics," 23rd AIA Computational Fluid Dynamics Conference, Conference, Location, 2017,

[3] Fife, M., E.;Davis,R,L. "A Conjugate Heat Transfer RANS/DES Simulation Procedure," 47th AIAA Aerospace Sciences meeting including the new horizons forume and erospace exposition, Conference, Location, 2009,

[4] Reinert, J. D., Dwivedi, A., and Candler, G. V. "Verification of a conjugate heat transfer tool with US3D," AIAA Scitech 2019, Conference, Location, 2019. doi: 10.2514/6.2019-1892

[5] Seager, C., and Agarwal, R. K. "Hypersonic Blunt-Body Shape Optimization for Reducing Drag and Heat Transfer," *Journal of Thermophysics and Heat Transfer* Vol. 31, No. 1, 2017, pp. 48-55. doi: 10.2514/1.t4650

[6] Nordstrom, J., and Berg, J. "Conjugate heat transfer for the unsteady compressible Navier-Stokes equations using a multi-block coupling," *Computers & Fluids* Vol. 72, 2013, pp. 20-29. doi: 10.1016/j.compfluid.2012.11.018

[7] Errera, M. P., and Baque, B. "A quasi-dynamic procedure for coupled thermal simulations," *International Journal for Numerical Methods in Fluids* Vol. 72, No. 11, 2013, pp. 1183-1206. doi: 10.1002/fld.3782

[8] Dechaumphai, P., Thornton, E. A., and Wieting , A. R."Fluid-Thermal-structural Study of Aerodynamically Heated Leading Edges," NASA Technical Memorandum, NASA, Langley Research Center , Hampton, Virginia, 1988.

[9] Zhao, X., Sun, Z., Tang, L., and Zheng, G. "Coupled Flow-Thermal-Structural Analysis of Hypersonic Aerodynamically Heated Cylindrical Leading Edge," *Engineering Applications of Computational Fluid Mechanics* Vol. 5, No. 2, 2011, pp. 170-179. doi: 10.1080/19942060.2011.11015361

[10] Maute, K., Nikbay, M., and Farhat, C. "Coupled analytical sensitivity analysis and optimization of three-dimensional nonlinear aeroelastic systems," *AIAA Journal* Vol. 39, No. 11, 2001, pp. 2051-2061. doi: 10.2514/2.1227

[11] Jameson, A."Aerodynamic Shape Optimization Using the Adjoint Method," Von Karman Institute, Brussels, 2003.

[12] Reuther, J., Jameson, A., Alonso, J., Jose, Rilinger, M., J, and Saunders, D."Constrained Multipoint Aerodynamic Shape Optimization Using an Adjoint Formulation and Parallel Computers," The Research Institute of Advanced Computer Science, 2018.

[13] Polle, D., Allen, C., and Rendall, T. "A Constrained Global Optimization FrameWork," 14th AIAA Aviation Technology , Integraiton, and operations conference, Conference, Location, 2014,

[14] Mavriplis, D. J., Fabiano, E., and Anderson, E. "Recent Advances in High-Fidelity Multidisciplinary Adjoint-Based Optimization with the NSU3D Flow Solver Framework," 55th AIAA Aerospace Sciences Meeting, Conference, Location, 2017. doi: 10.2514/6.2017-1669

[15] Newman, J. C., Taylor, A. C., Barnwell, R. W., Newman, P. A., and Hou, G. J. W. "Overview of sensitivity analysis and shape optimization for complex aerodynamic configurations," *Journal of Aircraft* Vol. 36, No. 1, 1999, pp. 87-96. doi: 10.2514/2.2416

[16] Nielsen, E. J., and Anderson, W. K. "Aerodynamic design optimization on unstructured meshes using the Navier-Stokes equations," *AIAA Journal* Vol. 37, No. 11, 1999, pp. 1411-1419. doi: 10.2514/2.640

[17] Mavriplis, D. J. "Discrete Adjoint-Based Approach for Optimization Problems on Three-Dimensional Unstructured Meshes," *AIAA Journal* Vol. 45, No. 4, 2007, pp. 741-750. doi: 0.2514/1.22743

[18] Mishra, A., Mani, K., Mavriplis, D. J., and Sitraman, J. "Time Dependent Adjoint-based Optimization for Coupled Aeroelastic Problems," 21st AIAA CFD Conference, Conference, Location, 2013,

[19] Kenway , G. K. W., and Martins, J. "Multipoint High-Fedility Aerostructural Optimization of a Transport Aircraft Configuration," *Journal of Aircraft* Vol. 51, No. 1, 2014, pp. 144-160. doi: 10.2514/1.C032150

[20] Mavriplis, J., Dimitri."Formulation and Multigrid Solution of the Discrete Adjoint Problem on Unstructured Meshes," Engineering, D. o. M., University of Wyoming, Laramie, Wyoming, USA.

[21] Mavriplis, J., Dimitri."Time Dependent Adjoint Methods for Single and Multi-disciplinary Problems," Engineering, D. o. M., University of Wyoming, Laramie, Wyoming, USA, 2015.

[22] Kamali, S., Mavriplis, D. J., and Anderson, E. "Development and Validation of a High-Fidelity Aero-Thermo-Elastic Analysis Capability," AIAA SCITECH 2020 Forum, Conference, Location, 2020. doi: 10.2514/6.2020-1449

[23] Jaiman, R. K., Jiao, X., Geubelle, P. H., and Loth, E. "Assessment of conservative load transfer for fluid-solid interface with non-matching meshes," *International Journal for Numerical Methods in Engineering* Vol. 64, No. 15, 2005, pp. 2014-2038. doi: 10.1002/nme.1434

[24] Jiao, X. M., and Heath, M. T. "Common-refinement-based data transfer between non-matching meshes in multiphysics simulations," *International Journal for Numerical Methods in Engineering* Vol. 61, No. 14, 2004, pp. 2402-2427. doi: 10.1002/nme.1147

[25] Cebral, J., and Loehner, R. "Conservative load projection and tracking for fluid-structure problems," 34th Aerospace Science meething and exhibit, Conference, Location, 1996. doi: 10.2514/6.1996-797

[26] Cebral, J., and Lohner, R. "conservative load projection and tracking for fluid-structure problems," *AIAA Journal* Vol. 35, No. 4, 1997, pp. 687-692. doi: 10.2514/2.158

[27] Roe, B., Jaiman, R., Haselbacher, A., and Geubelle, P. H. "Combined interface boundary condition method for coupled thermal simulations," *International Journal for Numerical Methods in Fluids* Vol. 57, No. 3, 2008, pp. 329-354. doi: 10.1002/fld.1637

[28] Mavriplis, D. J., and Mani, K. "Unstructured Mesh Solution Techniques using the NSU3D Solver," 52nd Aerospace Sciences Meeting, Conference, Location, 2014. doi: 10.2514/6.2014-0081
[29] Mavriplis, D. J., Anderson, E., Fertig, R., and Garnish, M. "Development of a High-Fidelity Time-Dependent Aero-Structural Capability for Analysis and design," 57th AIAA/ASCE/AHS/ASC Structures, Structural Dynamics, and Materials Conference, AIAA SciTech Forum, Conference, Location, 2016. doi: 10.2514/6.2016-1175
[30] Vassberg, J. C., Tinoco, E. N., Mani, M., Zickuhr, T., Levy, D., Broderson, O. P., Eisfeld, B., Wahls, R. A., Morrison, J. H., Mavriplis, D. J., and Murayama, M. "Summary of the Fourth AIAA CFD Drag Prediction Workshop," AIAA, Conference, Location, 2010. doi: 10.2514/6.2010-4547
[31] Vassberg, J. C., Tinoco, E. N., Mani, M., Broderson, O. P., Eisfeld, B., Wahls, R. A., Morrison, J. H., Zickuhr, T., Laflin, K. R., and Mavriplis, D. J. "Abridged Summary of the Third AIAA Computational Fluid Dynamics Drag Prediction Workshop," *Journal of Aircraft* Vol. 45, No. 3, 2008, pp. 781-798. doi: 10.2514/1.30572
[32] Mavriplis, D. J., Yang, Z., and Long, M. "Results Using NSU3D for the First Aeroelastic Prediction Workshop," 51st AIAA Aerospace Sciences Meeting, Conference, Location, 2013. doi: 10.2514/6.2013-786
[33] Mavriplis, D. J., Long, M., Lake, T., and Langlois, M. "NSU3D Results for the Second AIAA High-Lift Prediction Workshop," 52nd AIAA Aerospace Sciences Meeting, Conference, Location, 2014. doi: 10.2514/6.2014-0748
[34] Anderson, E., Bhuiyan, F. H., Mavriplis, D. J., and Fertig, R. "Adjoint-Based High-Fidelity Aeroelastic Optimization of Wind Turbine Blade for Load Stress Minimization," Wind Energy Symposium, AIAA SciTech Forum Conference, Location, 2018. doi: 10.2514/6.2018-1241
[35] Mavriplis, D. J., Yang, Z., and Anderson, E. "Adjoint Based Optimization of a Slotted Natural Laminar Flow Wing for Ultra Efficient Flight," AIAA SCITECH 2020 Forum, Conference, Location, 2020. doi: 10.2514/6.2020-1292
[36] Mavriplis, D. J. "Solution of the Unsteady Discrete Adjoint for Three-Dimensional Problems on Dynamically Deforming Unstructured meshes," Proceedings of the 46th Aerospace Sciences Meeting and Exhibit, Conference, Location, 2008. doi: 10.2514/6.2008-727
[37] Mani, K., and Mavriplis, D. J. "Geometry Optimization in Three-Dimensional Unsteady Flow Problems using the Discrete Adjoint," 51st AIAA Aerospace Sciences Meeting, Conference, Location, 2013. doi: 10.2514/6.2013-662
[38] Roe, P. L. "Approximate Riemann Solvers Parameter Vectors and Difference Schemes," *Journal of Computational Physics* Vol. 43, No. 2, 1981, pp. 357-372. doi: 10.1016/0021-9991(81)90128-5
[39] Barth, T., and Jespersen, D. "The design and application of upwind schemes on unstructured meshes," 27th Aerospace Sciences Meeting, Conference, Location, 1989. doi: 10.2514/6.1989-366
[40] Mani, K., and Mavriplis, D. J. "Adjoint-Based Sensitivity Formulation for Fully Coupled Unsteady Aeroelasticity Problems," *AIAA Journal* Vol. 47, No. 8, 2009, pp. 1902-1915. doi: 10.2514/1.40582
[41] Anderson, E."Development of an Open-Source Capability for High-Fidelity Thermoelastic Modeling and Adjoint-Based Sensitivity Analysis of Structures," Ph.D Dissertation, Mehcnaical Engineering, university, Laramie, Wyoming, 2019.
[42] "Abaqus," Version 6.14-4 ed., product of Dassault Systems Simulia Corp, Providence,RI,USA, 2017.
[43] Hilber, H. M., Hughes, T. J. R., and Taylor, R. L. "Improved Numerical Dissipation for Time Integratoin Algorithms in Structural Dynamics," *Earthquake Engng Struct. Dynamics* Vol. 5, 1977, pp. 283-292. doi: 10.1002/eqe.4290050306
[44] Nocedal, J., and Wright, S. *Numerical Optimization*, Springer, Verlag, NY, 1999.
[45] Samareh, J., A. "Discrete Data Transfer Technique for Fluid-Structure Interaction," 18th AIAA Computational Fluid Dynamics Conference, Conference, Location, 2007. doi: 10.2514/6.2007-4309
[46] Verstraete, T., Alsalihi, Z., and Van den Braembussche, R. A. "Numerical Study of the Heat Transfer in Micro Gas Turbines," *Journal of Turbomachinery* Vol. 129, No. 4, 2007, p. 835. doi: 10.1115/1.2720874
[47] Verstraete, T., Alsalihi, Z., and Van den Braembussche, R. A. "A comparison of conjugate heat transfer methods applied to an axial helium turbine," *Proceedings of the Institution of Mechanical Engineers, Part A: Journal of Power and Energy* Vol. 221, No. 7, 2007, pp. 981-989. doi: 10.1243/09576509jpe385
[48] Giles, M. B. "Stability analysis of numerical interface conditions in fluid-structure thermal analysis," *International Journal for Numerical Methods in Fluids* Vol. 25, No. 4, 1997, pp. 421-436. doi: 10.1002/(Sici)1097-0363(19970830)25:4<421::Aid-Fld557>3.0.Co;2-J
[49] Joshi, O., and Leyland, P. "Stability Analysis of a Partitioned Fluid–Structure Thermal Coupling Algorithm," *Journal of Thermophysics and Heat Transfer* Vol. 28, No. 1, 2014, pp. 59-67. doi: 10.2514/1.t4032
[50] Roget, B., and Sitaraman, J. "Wall distance search algorithm using voxelized marching spheres," *Journal of Computational Physics* Vol. 241, 2013, pp. 76-94. doi: 10.1016/j.jcp.2013.01.035
[51] Donea, J., Huerta, A., and Ponthot, J. *Encyclopedia of Computational Mechanics*, 2004.
[52] Miller, B., A."Loosely Coupled Time Integration of Fluid-Thermal-Structural Interactions in Hypersonic Flows," Ph.D Dissertation, Aeronautical and Astronautical Engineering, university, 2015.
[53] Thomas, P., D., and Lombard, C., K. "Geometric Consevation Law and its Application to Flow Computations on Moving Grids," *AIAA Journal* Vol. 17, No. 10, 1970, pp. 1030-1037. doi: 10.2514/3.61273
[54] Yang, Z., and Mavriplis, D. J. "A Mesh Deformation Strategy Optimized by the Adjoint Method on Unstructured Meshes," 45th AIAA Aerospace Sciences Meeting and Exhibit, Conference, Location, 2007. doi: 10.2514/6.2007-557
[55] Yang, Z., and Mavriplis, D. J. "Higher-Order Time Integration Schemes for Aeroelastic Applications on Unstructured Meshes," *AIAA Journal* Vol. 45, No. 1, 2007, pp. 138-150. doi: 10.2514/1.22847

[56] Mani, K."Application of Discrete Adjoint Method to Coupled Multidisciplinary Unsteady Flow Problems for Error Estimation and Optimization," Doctor of Philosophy, Department of Mechanical Engineering, university, Laramie, Wyoming, 2009.
[57] Fabiano, E."Multidisciplinary Adjoint-based Optimization Technicques for Helicopter Rotrs " Doctor of Philosophy, Department of Mechanical Engineering, university, Laramie, Wyoming.
[58] Newman, C., James III, Anderson, W. K., and Whitfield, D. L."Multidisciplinary Sensitivity Derivatives Using Complex Variables," Computational Fluid Dynamics Laboratory, N. E. R. C. f. C. F. S., Mississippi State University, Mississipi, USA, 1998.
[59] Thornton, E., and Dechaumphai, P. "Coupled flow, thermal and structural analysis of aerodynamically heated panels," 1987. doi: 10.2514/6.1987-700
[60] Shi, S., Dai, C., and Wang, Y. "Design and optimization of an integrated thermal protection system for space vehicles," 20th AIAA International Space Planes and Hypersonic Systems and Technologies Conference, Conference, Location, 2015. doi: 10.2514/6.2015-3553
[61] Thornton, E., and Dechaumphai, P. "Finite element prediction of aerothermal-structural interaction of aerodynamically heated panels," 1987. doi: 10.2514/6.1987-1610
[62] Thornton, E., A., and Dechaumphai , P. "Coupled Flow, Thermal, and Structural Analysis of Aerodynamically Heated Panels," *Journal of aircraft* Vol. 25, No. 11, 1988. doi: 10.2514/3.45702